




2022

METABOLIC DIVERSITY AMONG FIBROBLASTS FROM REGENERATING AND NON-REGENERATING MAMMALS

Ebenezer Aryee

University of Kentucky, enar227@uky.edu

Author ORCID Identifier:

 <https://orcid.org/0000-0002-3703-0559>

Digital Object Identifier: <https://doi.org/10.13023/etd.2022.238>

[Right click to open a feedback form in a new tab to let us know how this document benefits you.](#)

Recommended Citation

Aryee, Ebenezer, "METABOLIC DIVERSITY AMONG FIBROBLASTS FROM REGENERATING AND NON-REGENERATING MAMMALS" (2022). *Theses and Dissertations--Biology*. 86.
https://uknowledge.uky.edu/biology_etds/86

This Master's Thesis is brought to you for free and open access by the Biology at UKnowledge. It has been accepted for inclusion in Theses and Dissertations--Biology by an authorized administrator of UKnowledge. For more information, please contact UKnowledge@lsv.uky.edu.

STUDENT AGREEMENT:

I represent that my thesis or dissertation and abstract are my original work. Proper attribution has been given to all outside sources. I understand that I am solely responsible for obtaining any needed copyright permissions. I have obtained needed written permission statement(s) from the owner(s) of each third-party copyrighted matter to be included in my work, allowing electronic distribution (if such use is not permitted by the fair use doctrine) which will be submitted to UKnowledge as Additional File.

I hereby grant to The University of Kentucky and its agents the irrevocable, non-exclusive, and royalty-free license to archive and make accessible my work in whole or in part in all forms of media, now or hereafter known. I agree that the document mentioned above may be made available immediately for worldwide access unless an embargo applies.

I retain all other ownership rights to the copyright of my work. I also retain the right to use in future works (such as articles or books) all or part of my work. I understand that I am free to register the copyright to my work.

REVIEW, APPROVAL AND ACCEPTANCE

The document mentioned above has been reviewed and accepted by the student's advisor, on behalf of the advisory committee, and by the Director of Graduate Studies (DGS), on behalf of the program; we verify that this is the final, approved version of the student's thesis including all changes required by the advisory committee. The undersigned agree to abide by the statements above.

Ebenezer Aryee, Student

Dr. Ashley W. Seifert, Major Professor

Dr. Jessica C. Santollo, Director of Graduate Studies

METABOLIC DIVERSITY AMONG FIBROBLASTS FROM REGENERATING AND
NON-REGENERATING MAMMALS

THESIS

A thesis submitted in partial fulfillment of the
requirements for the degree of Master of Science in the
College of Arts and Sciences
at the University of Kentucky

By

Ebenezer Nii Adama Aryee

Lexington, Kentucky

Director: Dr. Ashley W Seifert, Associate Professor of Biology

Lexington, Kentucky

2022

Copyright © Ebenezer Aryee 2022

<https://orcid.org/0000-0002-3703-0559>

ABSTRACT OF THESIS

METABOLIC DIVERSITY AMONG FIBROBLASTS FROM REGENERATING AND NON-REGENERATING MAMMALS

Regeneration is a wound repair process that terminates in the restoration of tissue function and structure. Fibroblasts play pivotal roles in regenerative and fibrotic wound repair. Reports of extensive regenerative ability in mammals have been historically rare, but more recently spiny mice (*Acomys*) have emerged as a bona fide model of complex tissue regeneration. Recent work has indicated that fibroblasts from regenerators (*Acomys* and *Oryctolagus*) are more resistant to reactive oxygen species (ROS)-induced senescence compared to non-regenerating species, suggesting the influence of intrinsic cellular states on the fate of wound repair. Determining the basal metabolic signature of fibroblasts in the wound microenvironment, which experiences drastic changes in pH, cytokine bursts, hypoxia, damage associated molecular patterns (DAMPs), ROS bursts, as well as an innate and adaptive immune response, is key to understanding the dichotomy in wound repair outcomes between regenerating and non-regenerating species. I made use of fibroblasts isolated from the ear pinna of sexually mature spiny mice (*Acomys cahirinus*) and laboratory mice (*Mus musculus*), since extensive tissue repair had been reported in the former and not in the latter. I hypothesized that the underlying metabolic signatures between the two species would differ significantly with respect to glycolytic flux: oxidative phosphorylation (OxPHOS) rate ratios, with *Mus* exhibiting higher OxPHOS flux and *Acomys* being comparably glycolytic. In this study we show that under basal conditions in vitro, fibroblasts from *Acomys* possess a glycolytic bias compared to fibroblasts from *Mus*. In response to chronic glucose starvation, *Acomys* fibroblasts show no significant changes in glycolytic or OxPHOS rates, whereas *Mus* fibroblasts respond with significant increases in glycolytic and OxPHOS rates under similar conditions. In a bid to determine if glutamine metabolism played a pivotal role in maintaining this metabolic state in *Acomys*, we observed that treatment with BPTES (a glutamine metabolism inhibitor) caused mostly insignificant reductions in OxPHOS and glycolytic flux rates in both species, while DMSO exposure caused *Acomys* fibroblasts to switch their metabolic signature in response to glucose starvation, to one identical to *Mus*.

KEYWORDS: metabolism, regeneration, fibroblasts, glycolysis, oxidative phosphorylation

Ebenezer Nii Adama Aryee

(Name of Student)

04/20/2022

(Date)

METABOLIC DIVERSITY AMONG FIBROBLASTS FROM REGENERATING AND
NON-REGENERATING MAMMALS

By

Ebenezer Nii Adama Aryee

Ashley W. Seifert

Director of Thesis

Jessica C. Santollo

Director of Graduate Studies

04/20/2022

Date

DEDICATION

To ADONAI

Ataa-Naa Nyonmo

TsE Ofe

Gborbilor Kpanaku

Olowogbogboro.

To Elijah, Josiah, Jael, Angel, David, Ella, Eddie, Joel, and Sera; a new generation I hope would witness and largely benefit from the cumulative work done in this field of regenerative biology.

ACKNOWLEDGEMENTS

Regeneration biology is a field of research that seems almost phantasmal for someone with my background. I'm living out a dream, mental images I could only daydream about in high school. I want to appreciate Dr. Ashley Seifert for seeing the potential in me and giving me this opportunity. In addition, his role as a mentor in and outside the lab, sets quite a standard in scholarship and leadership that I can only aspire to. Drs. Duncan, Kikani, and Sullivan, members of my thesis committee, have also been of immense help and guidance throughout the journey.

My family both here and abroad have also been a strong support system for me over the years, especially my parents, Rev. Eddie, and Mrs. Patience Aryee. I would also like to appreciate Drs. Jonathan Adjimani, Lydia Mosi, and Patrick Arthur for stimulating and nurturing my passion for biochemistry cell, and molecular biology during my undergraduate studies.

Bench work acknowledgements go to Hemendra Vekaria, Aloysius Ajoy, and Sandeep Saxena, who trained me in the various assays used in this project. Special thanks also go to Dr. Sullivan for giving me access to his facilities and equipment. To my lab mates who created a helpful environment for growth and fun, I appreciate every high five, encouraging word and clarifying explanation.

TABLE OF CONTENTS

ACKNOWLEDGEMENTS iii

TABLE OF CONTENTS..... iv

LIST OF FIGURES vi

1. INTRODUCTION 1

2. MATERIALS AND METHODS 6

 2.1 Animals..... 6

 2.2 Tissue harvest, fibroblast isolation and in vitro culture. 6

 2.3 Immunocytochemistry 6

 2.4 MitoTracker Staining 7

 2.5 Microscopy & Image Acquisition..... 7

 2.6 Fibroblast Oxygen Consumption and Extracellular Acidification Measurement..... 8

 2.7 Mitochondrial Isolation, and Membrane Potential determination Assays 8

 2.8 BPTES treatment..... 8

 2.9 Statistical analyses. 9

3. RESULTS 10

 3.1.1 *Acomys* fibroblasts differ physiologically from *Mus* fibroblasts under basal conditions *in vitro*. 10

 3.1.2 Mitochondria from *Acomys* fibroblasts are large, and spherical whereas mitochondria from *Mus* fibroblasts are smaller and more abundant. 13

 3.1.3 Mitochondria isolated from *Acomys* and *Mus* fibroblasts differ in membrane potential levels 13

 3.2 Substrate starvation tests. 14

 3.2.1 Mitochondria from *Acomys* fibroblasts undergo substantial structural changes in response to glucose starvation, while *Mus* mitochondria change minimally in response to glucose starvation. 15

 3.2.2 *Acomys* fibroblasts do not show a significant metabolic response to glucose deprivation despite changes in mitochondrial phenotype..... 16

 3.2.3 *Acomys* fibroblasts do not show significant changes in glycolytic response following glucose administration to glucose starved cells. 18

 3.3 Glutamine metabolism inhibition experiments (within the scope of glucose deprivation)..... 19

 3.3.1 Within-specie comparisons of OCR parameters in response to BPTES treatment. 20

3.3.2 Across-specie comparisons of OCR parameters in response to BPTES treatment	22
3.3.3 Within-specie comparisons of ECAR parameters in response to BPTES treatment	23
3.3.4 Across-specie comparisons of ECAR parameters in response to BPTES treatment	25
3.3.5 <i>Acomys</i> fibroblasts mitochondria switch from a spherical to an elongated phenotype in response to glucose starvation and DMSO exposure.	27
3.3.6 Glucose availability and BPTES treatment do not have an effect on <i>Acomys</i> fibroblast survivability.....	27
4. DISCUSSION	29
APPENDIX A: Metabolic response to glucose removal over time.	35
BIBLIOGRAPHY	36
VITA.....	40

LIST OF FIGURES

Figure 1. ATP generation pathways in the cell.5

Figure 2. General mitochondrial and cellular description of *Mus* and *Acomys* fibroblasts in vitro.....10

Figure 3. Schematic for basal physiological characterization experiments.....11

Figure 4. *Acomys* and *Mus* fibroblasts show different Glycolytic and Oxidative phosphorylation phenotypes in vitro.12

Figure 5. Mitochondria from *Acomys* and *Mus* fibroblasts differ phenotypically and functionally.13

Figure 6. Mitochondria membrane potential in *Mus* fibroblasts trend higher compared to *Acomys*14

Figure 7. Schematic for glucose starvation experiments.15

Figure 8. Mitochondria from *Acomys* and *Mus* fibroblasts differ in their phenotypic response to glucose deprivation.16

Figure 9. *Acomys* fibroblasts resist glucose starvation-induced increases in oxidative phosphorylation.17

Figure 10. *Acomys* fibroblasts resist glucose starvation-induced increases in glycolytic flux18

Figure 11. Schematic for glutamine metabolism inhibition experiments.....20

Figure 12. Glutamine metabolism inhibition in the light of glucose availability elicits different responses in mitochondrial respiration in *Acomys* and *Mus* fibroblasts.....22

Figure 13. Glutamine metabolism inhibition in the light of glucose availability elicits different Glycolytic responses in *Acomys* and *Mus* fibroblasts.25

Figure 14. *Acomys* mitochondria dynamics are affected by glucose availability and DMSO exposure; BPTES treatment alters mitochondrial phenotype in *Mus* fibroblasts.....26

Figure 15. Glucose starvation and BPTES treatment do not have significant effect on cell survivability in *Acomys* fibroblasts.28

Figure 16. Key metabolic substrates produce and generate intermediates/products with anabolic, antioxidant and signaling functions.....33

1. INTRODUCTION

Cellular metabolism is the central feature for all life on earth. Metabolism can be anabolic or catabolic, with the latter focused on the breakdown of substrates, externally or internally sourced to generate energy. Adenosine triphosphate (ATP), a building block for nucleic acid synthesis, also functions centrally as the unit of energy in biological systems. Although substrate forms and electron donors may differ (especially in the case of obligate anaerobes), ATP generation is the end goal. It is key to note that energy generation processes go beyond ATP generation, with multiple reports of metabolic pathway intermediates and by-products functioning as signaling molecules, epigenetic modulators, markers/mediators of cellular transformation, differentiation, and reprogramming (Folmes et al., 2011); (Panopoulos et al., 2012).

ATP is generated in the cell via two main mechanisms: glycolysis and oxidative phosphorylation. Glycolysis is a cytoplasmic glucose breakdown pathway that generates ATP as byproducts. After the generation of only two molecules of ATP per molecule of glucose in glycolysis (Substrate Level Phosphorylation), 2 molecules of pyruvate are obtained as an end product. After being transported into the mitochondrion, pyruvate is converted to acetyl coA through oxidative decarboxylation and enters the TCA cycle. Oxidative phosphorylation takes place in the electron transport chain (within the inner mitochondrial membrane) and makes use of the reducing equivalents (NADH, FADH₂) to generate ATP, using a tightly coupled, electron donation-mediated proton gradient. Most of the reducing equivalents used for generating ATP are obtained from the TCA cycle, a metabolic hub pivotal to mitochondrial function. Glucose, glutamine, and fatty acyl carnitine are the key substrates for OxPHOS mediated ATP generation (Figure 1). Acetyl coA, the key intermediate for entry into the TCA cycle is a downstream (oxidized) metabolite of two of the key metabolic substrates, glucose, and fatty acids. Glutamine contributes its quota to the TCA cycle through the anaplerotic injection of glutamine-derived α -ketoglutarate, a TCA cycle intermediate. Through oxidative phosphorylation 38 molecules of ATP can be generated from a single molecule of glucose, which is far more efficient than the 2 molecules of ATP generated solely from glycolysis.

It is therefore interesting to observe that some cells are able to ramp up glycolysis at the expense pyruvate generation for TCA entry via a process called the “Warburg effect” (first characterized in tumor cells) whereby even under aerobic conditions, proliferative cells favor fermentation (lactate production from pyruvate) over the Krebs cycle as the end point for glycolytic products. Despite the stark difference in ATP generation efficiency when compared to oxidative phosphorylation, aerobic glycolysis is advantageous to rapidly proliferating cells as this would increase biomolecule synthesis, while concurrently bypassing carbon loss through CO₂ release in the TCA cycle. In rapidly proliferating cells, glycolytic flux and glutaminolysis is ramped up, with the only difference being that this processes of glucose and glutamine breakdown is only partial, with an increased emphasis on the generation of biomolecule precursors over meeting the cells energy demands, especially in the case of glucose utilization (Newsholme, Crabtree, & Ardawi, 1985). Newsholme and his team indicated that these high rates may not just be for biomolecule

precursor or energy production only but may serve as intrinsic boosters of sensitivity to cell signaling cues in response to various stimuli as seen in PAMP-triggered lymphocyte proliferation (Newsholme et al., 1985).

Aside cell proliferation, these distinctive metabolic signatures are most pronounced during ontogeny, such that when compared to highly respiring or lowly respiring differentiated cells, stem cells (be it induced pluripotent stem cells (iPSCs) or embryonic stem cells (ESCs), show a higher dependence on glycolysis compared to O₂PHOS. The correlation between ontology and glycolytic bias becomes more intimately linked in the case of cellular reprogramming, where reprogramming efficiency of iPSCs to pluripotency is linked to a pro-glycolytic metabolic state, with efficiency increased and decreased significantly in response to glycolytic inhibitors and augmenters respectively (Folmes et al., 2011); (Panopoulos et al., 2012).

Transcription factor mediated reprogramming of differentiated cells to iPSCs triggers a change from the typical differentiated cell mitochondrial/oxidative stress pathways to one that alters intrinsic cellular senescence pathways (Prigione, Fauler, Lurz, Lehrach, & Adjaye, 2010), resulting in cells which are mirror images of ESCs with respect to pluripotency, gene expression, self-renewal, and morphology. It has been reported that the mitochondria within reprogrammed iPSCs do not maintain their somatic phenotype, but also transform to an ESC-like phenotype, with concurrent changes in mtDNA levels, mitochondrial biogenesis, lactate production, cytoplasmic ATP levels, among other metabolic parameters, and that upon differentiation, these parameters revert to the high O₂PHOS, senescence-prone differentiated cell state (Prigione et al., 2010). So far, most, if not all, metabolism studies across different cell types use three model species: humans, rats (*Rattus norvegicus*), and lab mice (*Mus musculus*). This underscores the need to study metabolism in other of model organisms where the potential to reveal alternate pathways may cast new light on outstanding questions in biomedical research.

Wound repair in animals is one result of tissue damage, with persisting ulceration a possible complication from incomplete or truncated wound repair. Even when successful, ie. re-epithelialization (wound closure) the structure and function of the repaired tissue lies within a spectrum. From simple scars to hypertrophic scars to keloids, wound repair may not necessarily bring about an expected result, in that the structure, and hence the function of the damaged tissue could be lost, causing disability. Right after an injury, hemostasis is followed by, inflammation, re-epithelialization, cell proliferation, new tissue production and tissue remodeling.

On the far end of the spectrum, is reparative regeneration, a complex set of biological operations that typically combines processes common to fibrotic repair and development, and one whose endpoint restores tissue structure and function, as reviewed by (Simkin & Seifert, 2018): (Aztekin & Storer, 2022). Despite centuries of study, extensive epimorphic tissue regeneration, was rarely reported in mammals. Epimorphic regeneration differs from hypertrophy and morphallaxis, in that it involves the formation of the blastema, a block of proliferating cells at the injury site within an environment

wrapped in a flurry of activity- varying bursts in cell signals (ROS, cytokines), cell migration, tissue remodeling, cellular de-differentiation and re-differentiation. Fibrotic repair and regeneration share many similarities in the initial stages of wound healing but also demonstrated differences with respect to the duration and extent of inflammation, cell proliferation and ECM remodeling efficiency resulting in different levels of structural and functional restoration of injured tissue (Seifert et al., 2012); (Gawriluk et al., 2016).

Spiny mice (*Acomys cahirinus*) are rodents found in arid and semi-arid regions of Africa, Asia, and the Middle East (Jeremy & Bates, 1994) that have been extensively researched for the study of diabetes, renal physiology, and even fetal development. Importantly, these precocial mice are recognized as a better model for human birth and pregnancy compared to altricial mice, as reviewed by (Sandoval & Maden, 2020). The regenerative abilities of *Acomys kempfi* and *Acomys percivali* were first reported as a response to skin autotomy, a rare feat in mammals. It was observed that instead of scarring, ear-punch injuries in these *Acomys* species resulted in complete restoration of the missing tissue: dermis, hair follicles, sweat glands and even cartilage (Seifert et al., 2012).

Building on this report and through research over the past decade, spiny mice and in particular the captive bred *Acomys cahirinus* have proved to be emerging models to study tissue regeneration of the skin (Seifert et al., 2012); (Maden, 2018), musculoskeletal tissue, muscle (Maden et al., 2018) kidney (Okamura et al., 2018) and even spinal cord injuries (Streeter et al., 2020); (Nogueira-Rodrigues et al., 2022). Spiny mice have been observed to carry out extensive tissue regeneration response to acute injury. While regeneration, is observed in urodeles, it is relatively rare in mammals with this difference among species conventionally explained by differences in the extent of inflammation and the presence and development of an innate and adaptive immune response (Lai et al., 2017); (Simkin, Gawriluk, Gensel, & Seifert, 2017). Comparative and gain-of-function studies have identified three primary factors that contribute to differences in regenerative ability between species: the wound environment (ECM, signaling environment-neurotransmitters, paracrine, signals) (Watt & Huck, 2013); (McCusker & Gardiner, 2013), the resident cells (Saxena, Vekaria, Sullivan, & Seifert, 2019) and the immune response (Gawriluk et al., 2020); (Lai et al., 2017; Simkin et al., 2017).

Fibroblasts mediate the progression of the last three stages of wound repair through wound contraction, collagen deposition and ECM re-organization, making their contribution to wound resolution pivotal as reviewed by (desJardins-Park, Foster, & Longaker, 2018). *Acomys* and *Oryctolagus* fibroblasts have been shown to be highly proliferative, with reticence to radiation and ROS-induced senescence compared to fibroblasts obtained from non-regenerators (Saxena et al., 2019). Since ROS generation and management is intimately linked to cellular metabolism, we hypothesized that ROS-reticent *Acomys* and *Oryctolagus* fibroblasts possess metabolic oxidative pathways which do not fit into the differentiated cell mold – a pro-glycolytic profile (unusual for differentiated cells), which may prime them to receive wound site signals and respond

towards a regenerative phenotype. This metabolic state would be a stark contrast to the high OxPHOS state observed in fibroblasts from non-regenerators such as *Mus* and *Rattus*.

The relevance of these differences, hinges on their potential to effect the cellular response to similar signals in the wound environment, especially the high ROS burst that occurs shortly after injury (Niethammer, Grabher, Look, & Mitchison, 2009); (van der Vliet & Janssen-Heininger, 2014); (Simkin et al., 2017). Showing increased reticence to ROS-induced senescence, based on high antioxidant activity is a characteristic typical of highly proliferative cells (and stem cells), which undergo high levels of aerobic glycolytic flux. This process supports anabolism, with a marked reduction in ROS production, as well as biomolecule loss through CO₂ release via the TCA cycle as reviewed by (Zhang, Nuebel, Daley, Koehler, & Teitell, 2012). Again, understanding the intrinsic metabolic state of these resident tissue cells would help paint a better picture of how these fibroblasts may be primed to respond to wound injury signals, (which may be similar to that observed in non-regenerators) towards a pro-regenerative over a fibrotic response as seen in proliferative, high collagen I-spewing, scarring fibroblasts in non-regenerating mammals, like mice, rats, and humans.

Here, we show that *Acomys* fibroblasts show a pro-glycolytic metabolic state compared to *Mus* fibroblasts, which show a comparatively higher OxPHOS state. In addition, glucose starvation, which is expected to increase the oxidative phosphorylation: glycolytic flux ratio in cultured cells, didn't cause a significant increase in oxidative phosphorylation and glycolytic rate in *Acomys* fibroblasts, despite a noticeable change in mitochondrial phenotype. These observations suggested a plastic, highly compensatory metabolic state in *Acomys* fibroblasts, unlike what was seen in *Mus* fibroblasts, which showed exaggerated metabolic responses to chronic glucose deficiency. Experiments involving glutamine metabolism inhibition in the light of glucose availability showed decreases in oxygen consumption in both species in response to BPTES (a glutamine metabolism enzyme inhibitor) treatment. Interestingly, we show that *Acomys* fibroblasts lose their plasticity towards glucose deficiency, when exposed to DMSO, such that oxygen consumption rates outcompete those seen in *Mus* fibroblasts under similar conditions.

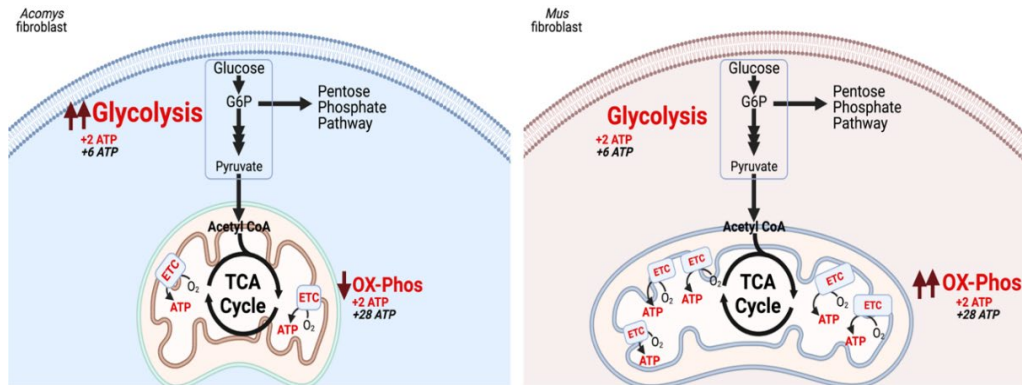
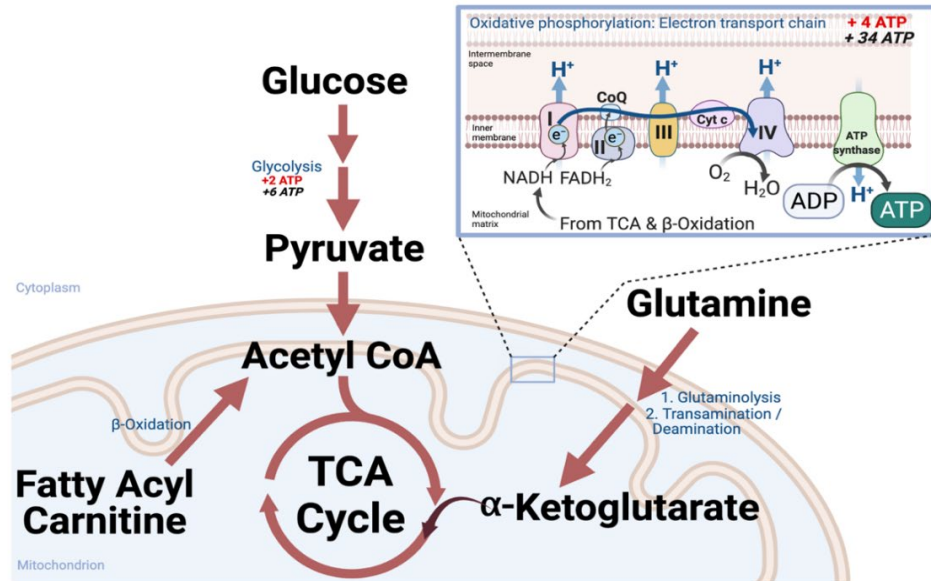


Figure 1. ATP generation pathways in the cell.

Fatty acids, glutamine and glucose are the main substrates for ATP generation in the cell (on top). Predictions for basal metabolic states of *Acomys* and *Mus* fibroblasts (bottom). Created with BioRender.com

2. MATERIALS AND METHODS

2.1 Animals

Outbred ND4 Envigo laboratory mice (*Mus musculus*) and African spiny mice (*Acomys cahirinus*) were kept and bred in the Seifert Lab animal housing building on the University of Kentucky Campus in Lexington. While *Mus* were only fed mouse chow (Tekland Global 2014, Harlan Laboratories, Indianapolis, IN), *Acomys* were fed 14% protein mouse chow and black-oil sunflower seeds (Pennington Seed Inc., Madison, GA) in a 3:1 ratio. Sexually mature adult mice and spiny mice were used for the study with the subjects sex matched in both species every time samples were harvested for each experiment. Tissue harvest entailed 4 mm biopsy punches (Sklar Instruments, West Chester, PA) created holes in the centers of the right and left ear pinnas. All animals were anaesthetized with 3% vaporized isoflurane (v/v) (Henry Schein Animal Health, Dublin, OH) at 1 psi oxygen flow rate. The University of Kentucky Institutional Animal Care and Use Committee (IACUC) approved all animal work described in this project under protocol 2013-1119.

2.2 Tissue harvest, fibroblast isolation and in vitro culture.

4mm full-thickness tissue biopsies were obtained from the centers of the ear pinnas of adult (12-week-old) *Mus musculus* and *Acomys cahirinus*. The tissues from each animal were pooled into separate 1.5 ml Eppendorf tubes. Single-cell suspensions were obtained via enzymatic (Trypsin-Dispase/Collagenase IV) and mechanical digestion (razor dicing/70 μ m filtering) steps. The suspension was pelleted and the cell pellets re-suspended and cultured in complete DMEM (10% FBS (Hyclone), and 1% Antibiotic-Antimycotic (Gibco), at 37⁰C under 3% O₂ and 5% CO₂ conditions in 10 cm plates. The cells were cultured and passaged at ~80% confluency, with each subsequent passage seeded with 200 000 cells in a 10 cm plate. During passaging steps, cells were counted using a hemocytometer.

2.3 Immunocytochemistry

EdU, DAPI, and γ H2AX staining was carried out on fibroblasts cultured up to the second passage. These P2 cells from both species were seeded on coverslips in 24-well plates at densities of 5000 cells per well. The fibroblasts were cultured at 37⁰C under 3% O₂ and 5% CO₂ conditions up until 45 hours. At the 45th hour, the media in the 24-well plates was replaced with EdU-Media mix (10 μ M EdU/DMEM), and the cell returned to the incubator for 3 more hours. At the 48th hour, the media was removed and the cells washed with PBS. The fibroblasts were then fixed with 10% formalin for 10 minutes, and the fixed cells washed 3 times with PBS at 5 minutes/wash. After washing, the fixed fibroblasts were permeabilized with 0.5% Triton X (5 μ l/1 ml PBS) for 20 minutes and then washed twice with PBS at 2 minutes/wash. The fixed fibroblasts were incubated with EdU solution (2M Tris, 50mM CuSO₄, Alexa Fluor azide, 0.5 M Ascorbic acid) in the dark for 30 minutes after which the solution was removed and the cells washed thrice with PBS

at 3 minutes/wash. The wells were blocked with secondary antibody serum (15 μ l/1ml PBS) for 30 minutes. After blocking, the wells were incubated with the primary antibodies (Vimentin and γ -H2AX; 1 μ l:500 μ l blocking solution) overnight at 4⁰C. After incubation the coverslips in the wells were washed thrice with PBS at 3 minutes/wash. The cells were then incubated with secondary antibody for 30 minutes at room temperature. After secondary antibody incubation, the cells were washed thrice with PBS at 5 minutes/wash, and DAPI (Invitrogen; 1:2000) applied for 15 minutes. After DAPI application, the cells were finally washed with DI H₂O for 1 minute, dried and the coverslips mounted on glass slides with Prolong Gold antifade reagent (Invitrogen). The primary antibody used was γ H2AX at 1:500 (rabbit mAb, P-H2A.X-Ser139, clone 20E3, Cell signaling technology). Secondary antibodies used were Donkey anti-rabbit Alexa flour 594 (A21207, Life technology, 2 mg/ml, 1:500), and Donkey anti-rabbit Alexa flour 488 (2 mg/ml, Invitrogen, 1:500). Cells positive for the individual markers were quantified using ~5 images captured at 20X magnification per sample, using an Olympus BX53 microscope with each image containing approximately 50 cells. With DAPI as a basal marker for all cells, marker-positive cells were quantified as a portion of all distinct DAPI positive zones.

2.4 MitoTracker Staining

For the detection of a concurrent effect of glucose deprivation on fibroblast mitochondrial phenotype via MitoTracker red staining, fibroblasts in both species under both conditions were seeded into 24 well plates on cover slips at 5000 cells per well and cultured for 48 hours. The media in the wells was removed, the cells washed with HBSS, and then incubated with MitoTracker (M7512, ThermoFisher scientific) staining media mix (0.3 μ l staining stock/ 1 ml FBS-free DMEM) for 30 minutes. After incubation, the cells were washed twice with PBS, and then fixed for 15 minutes in the dark with warm 4% formaldehyde. The 4% formaldehyde was removed after fixing and the fixed cells washed twice with PBS at 5 minutes/wash. Chilled acetone was added to the cells at 500 μ l/well and incubated for 5 minutes, after which it was removed, and the cells washed once with PBS. DAPI (1:2000/ HBSS) was added to each well and incubated for 15 minutes. The DAPI solution was removed, and the cells finally washed with DI H₂O. The coverslips were then air dried and mounted on glass slides with Prolong Gold antifade reagent (Invitrogen).

2.5 Microscopy & Image Acquisition

Manual characterization of mitochondrial phenotypes in both species was carried out using 40X fluorescent images taken using a BX53 microscope (Olympus, Tokyo, Japan) with a DP80 color camera on cellSens software (cellSens v1.12, Olympus Corporation). The same equipment was used in characterizing levels of senescence in cultured cells utilizing 20X fluorescent images using the DAPI, FITC and TEXAS RED channels for detecting nuclei, DNA strand breaks (γ H2AX) and DNA replication (EdU) respectively. In both sets of experiments, cells used were cultured on coverslips in 24 well plates and fixed before imaging. 40X images were used for characterizing mitochondrial

phenotypes with ~8 images taken per sample (n=3/species) with >30 cells counted per sample. 20X images were taken for senescence detection with ~4 images taken per sample and >120 cells counted per sample (n=3/species).

2.6 Fibroblast Oxygen Consumption and Extracellular Acidification Measurement

Measurements of cellular mitochondrial function, and glycolytic flux in the two fibroblast classes, under combinations of the 3 different conditions: control, glucose deficient, and BPTES-treated were taken with the XF Cell Mito Stress Test Assay Kit (Agilent Technologies) and XF Glycolysis Stress Test Kit (Agilent Technologies) respectively, using the Seahorse Bioscience XF96 Flux Analyzer. With three biological replicates and three technical replicates for each cell line per specie, the cells were seeded at passage two into the 96-well Seahorse culture plate at 30,000 cells per well. Glycolytic stress tests, utilizing glucose, Oligomycin and 2-DG, and Mitochondrial stress tests utilizing ETC inhibitors (Oligomycin, FTTP, Rotenone and Antimycin A) were run 18-24 hours after seeding on live cells, per the protocol provided by the manufacturer. From the MST, OCR parameters such as proton leak, maximal respiration, basal respiration, and ATP-linked respiration were quantified, while glycolysis, glycolytic capacity, non-glycolytic acidification, and glycolytic reserve were calculated using the Seahorse system.

2.7 Mitochondrial Isolation, and Membrane Potential determination Assays

Cultured fibroblasts were dislodged with (at P2) and spun down (1500 rpm for 5 minutes) after the reaction was stopped after 5 minutes with FBS-containing DMEM. The supernatant was poured off and the pellet kept on ice. 1 ml of Mito Isolation Buffer was added to the pellet and the pellet re-suspended. The suspension was spun at 400 rcf for 5 minutes, after which the supernatant was taken out and 450 μ l of EDTA added to the pellet and re-suspended. The samples were then broken up using a Nitrogen cell disruptor (1250psi for 10 minutes). The samples cell lysates were passed twice through a 26-gauge syringe, topped up with 1.5 ml of Mito Isolation Buffer, spun at 1300xg for 3 minutes at 4⁰C and the supernatant transferred into new tubes. These were then spun at 4⁰C at 1300xg this time for 10 minutes. The mitochondria were then spun down in a Ficoll gradient and quantified using a BSA assay. TMRE Assay was run and fluorescence was detected and measured by a plate reader on an opaque 96-well plate using 8 μ g of mitochondria per sample.

2.8 BPTES treatment

Bis-2-(5-phenylacetamido-1,3,4-thiadiazol-2-yl)ethyl sulfide was sourced from Tocris (5301). Fibroblasts were cultured under standard conditions (3% O₂, 5% CO₂, 37⁰C) up until P2. P2 cells were seeded into 24-well, and 96-well Seahorse culture plates at densities of 5000 and 40000 cells per well respectively. The adhered cells were exposed to 10 μ M for 4 hours before Mito tracker staining, Edu/DAPI/ γ -H2AX staining (coverslip

24-well plate), and MST and GST (96-well Seahorse culture plate), as described above. The cells grown in 4 conditions: Control (DMSO + Complete DMEM), BPTES + Glucose deficient DMEM, BPTES + Complete DMEM. Fixed cells from all treatments were prepared for immunocytochemistry as outlined above.

2.9 Statistical analyses.

JMP (version Pro 14.1.0, SAS Institute Inc.) was used to perform all statistical analyses. All Seahorse Assay results were analyzed using ANOVA (2-group for Glucose starvation experiments: species/conditions, 3-group for glutamine metabolism inhibition experiments: treatment/species/conditions) and pairwise comparisons made with the Tukey method. Significance for all statistical analyses done was set at $\alpha=0.05$.

3. RESULTS

3.1.1 *Acomys* fibroblasts differ physiologically from *Mus* fibroblasts under basal conditions *in vitro*.

Primary ear fibroblasts were isolated from sexually mature, 3-month-old *Acomys cahirinus* and *Mus musculus* (n=3/specie). Cellular suspensions were obtained in a process involving enzymatic (trypsin/dispase/collagenase) and mechanical digestion stages. Fibroblasts were cultured in complete DMEM and passaged twice. Using these cells, we used Mitotracker Red and DAPI to characterize mitochondrial morphology (Figure 2). Whereas *Acomys* fibroblasts exhibited relatively small cytoplasmic areas containing large spherical mitochondria (Figure 5a), *Mus* fibroblasts were much more heterogeneous whereby cells varied significantly in cell size, nuclear size and cytoplasmic extensions (Figure 2). *Acomys* on the other hand had relatively smaller cytoplasmic areas, with large spherical mitochondria positioned around the nucleus. Heterochromatin in *Mus* nuclei was notably pronounced, while *Acomys* nuclei did not show densely stained DNA characteristic of mouse cells. In fact, this characteristic was so distinct, cells from both species could be blindly identified.

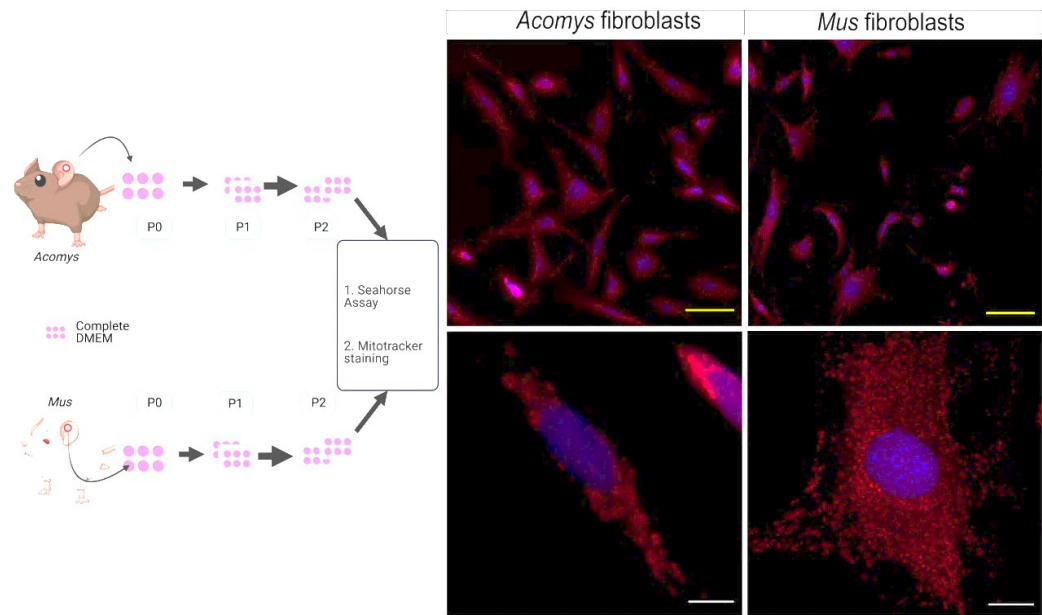


Figure 2. General mitochondrial and cellular description of *Mus* and *Acomys* fibroblasts in vitro.

Scale bars (white): 10 μm. Scale bars (yellow): 50 μm. Schematic created with BioRender.com

Next, we used a Seahorse Fe96x Metabolic Flux Assay to measure intrinsic Oxygen consumption rate (OCR) and Extracellular Acidification Rate (ECAR) in order to quantify oxidative phosphorylation and glycolytic flux respectively (Figure 4 a-d). Previous work indicated that *Acomys* fibroblasts had lower oxidative phosphorylation levels that remained significantly unchanged in response to ROS exposure (Saxena et al., 2019). Using passage

two fibroblasts, we observed significant differences in ECAR and OCR parameters in ECAR and OCR parameters between the two species when cultured in complete DMEM. *Acomys* fibroblasts, showed significantly higher ECAR parameters compared to *Mus* fibroblasts (Figure 4a-b) (glycolysis (ANOVA, $F= 29.7268$, $P = 0.0258$, 95% CI: 4.4 to 60.3), and glycolytic capacity (ANOVA $F= 28.3138$, $P = 0.0304$, 95% CI: 4.23 to 76.18). Glycolytic capacity measures the maximum rate of direct ATP generation from glycolysis. Although non-glycolytic acidification was higher in *Acomys*, this difference was not significant (ANOVA, $F= 5.9723$, $P = 0.0793$), per our set cut off at $\alpha=0.05$. This trend was observed in glycolytic reserve levels (ANOVA $F=, 10.9105$, $P = 0.2136$) (Figure 4a-b). Glycolytic reserve describes the intrinsic ability to respond to an energetic demand (simulated by Oligomycin) and belies the glycolytic flexibility of the cell and is calculated by subtracting glycolysis from glycolytic capacity (see Figure 3 lower right insert).

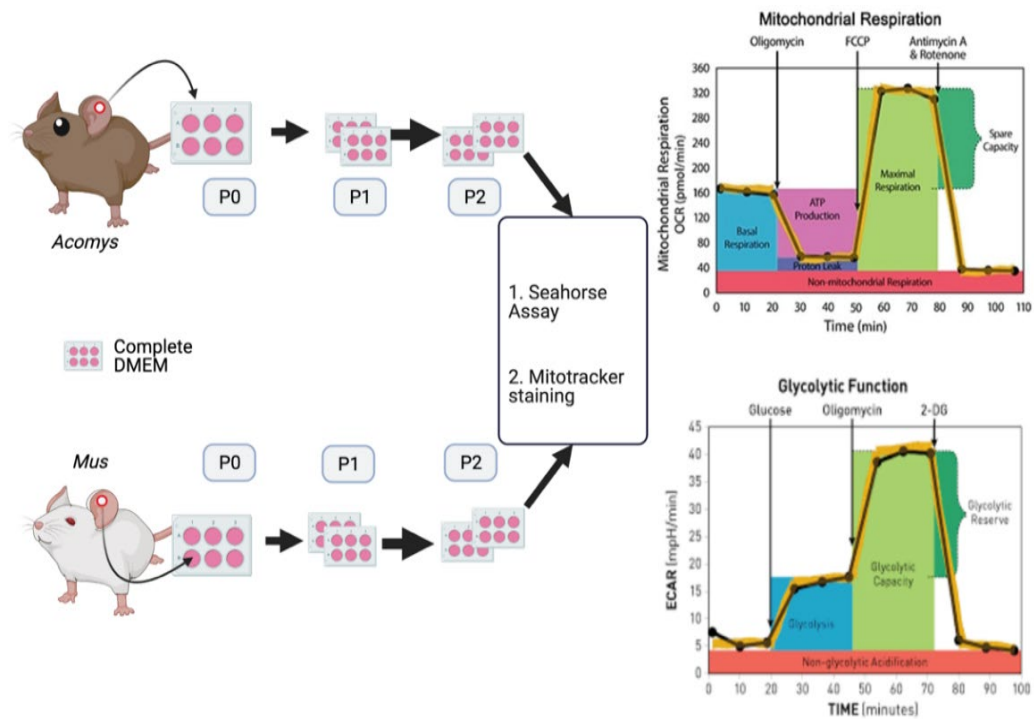


Figure 3. Schematic for basal physiological characterization experiments
Created with BioRender.com. Graphs acquired from Agilent technologies.

Mus fibroblasts showed significantly higher OCR parameters compared to *Acomys* with the exception being proton leak, where the difference between the two species was negligible ($P = 0.9999$) (Figure 4c-d) (basal respiration (ANOVA, $F= 15.1043$, $P= 0.0398$, 95% CI: -47.68 to -1.24), maximal respiration (ANOVA, $F= 28.8290$, $P < 0.0001$, 95% CI: -191.80 to -106.82), and spare respiratory capacity (ANOVA, $F= 28.4594$, $P < 0.0001$, 95% CI: -143.24 to -96.25). Basal respiration represents the cells basal energetic demands in the absence of any treatment or inhibitor. Maximum respiration gauges the maximal ability of

the cell to consume oxygen in a situation the energy demand of the cell is at its highest. This highest possible energy demand is simulated by FCCP, an electron transport chain uncoupler, which triggers explosive substrate oxidation (amino acids, fats, and sugars) to cater to this “energy demand”. Spare respiratory capacity describes the cell’s intrinsic ability to respond acutely to a sudden energy demand and measures the amount of extra ATP produced because of the FCCP-simulated energy demand and may be used as a predictor of cell fitness. It is calculated by subtracting Basal respiration from maximal respiration (see Figure 3 upper insert). Proton leak describes the portion of basal respiration which is uncoupled to ATP generation and can be used as a marker of mitochondrial impairment or can be used as a mitochondrial ATP generation modulating mechanism.

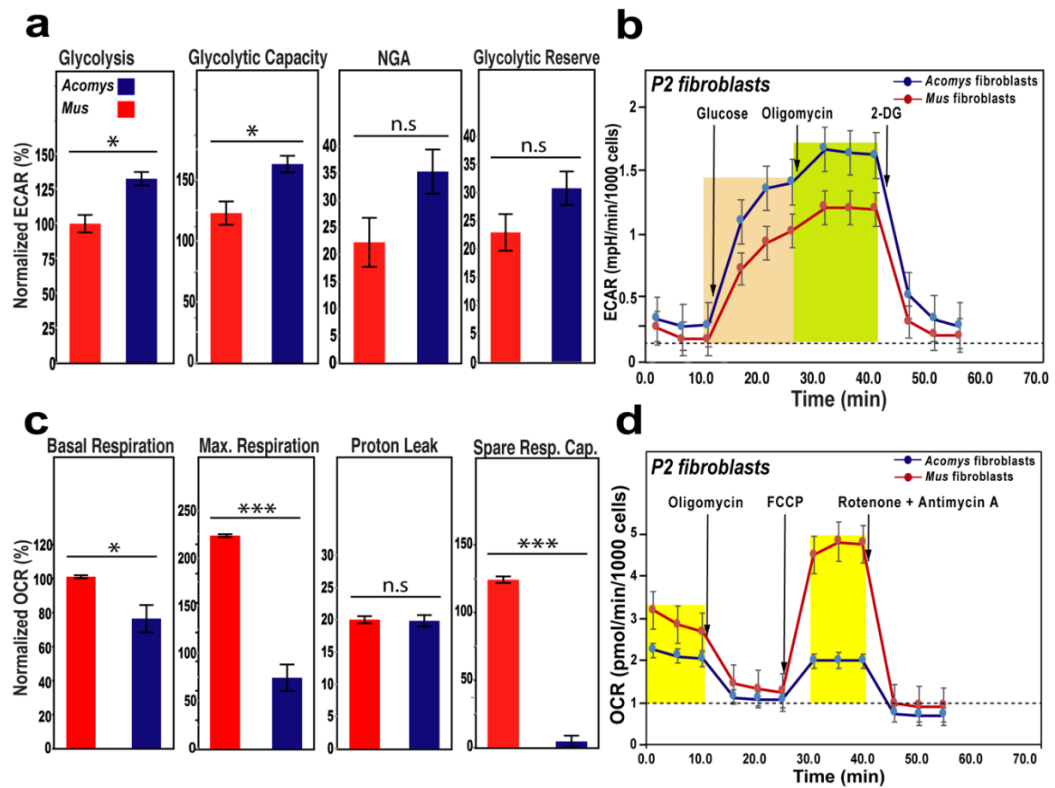


Figure 4. *Acomys* and *Mus* fibroblasts show different glycolytic and oxidative phosphorylation phenotypes in vitro.

ECAR parameters: Glycolysis, glycolytic capacity, proton leak and spare respiratory capacity were measured and compared between both species (a). ECAR test time course conducted on an XF94 analyzer on *Acomys* and *Mus* fibroblasts (b). OCR parameters: Basal respiration, Maximal respiration, Proton leak and Spare respiratory capacity were measured and compared between both species (c). OCR test time course conducted on an XF94 analyzer on *Acomys* and *Mus* fibroblasts (d). n=3/species. Measured ECAR and OCR were converted to percent normalized ECAR and OCR respectively. FCCP: Carbonyl cyanide-p-trifluoromethoxy phenyl hydrazone. 2-DG = 2-deoxy-glucose. Error bars= ±S.E.M.

3.1.2 Mitochondria from *Acomys* fibroblasts are large, and spherical whereas mitochondria from *Mus* fibroblasts are smaller and more abundant.

Based on our metabolic characterization of fibroblasts from *Acomys* and *Mus*, we next sought to better characterize mitochondrial phenotype in cells from both species. *Acomys* mitochondria presented as massive “doughnut”-like spheres (Figure 5a). However most mitochondria in *Mus* fibroblasts were also spherical ($88 \pm 4.4\%$ of cells) but were significantly smaller in size (Figure 2 and Figure 5b-c) Some mitochondria in *Mus* were hybrid ($10 \pm 2.9\%$ of cells) and a few were elongated ($2 \pm 1.7\%$ of cells).

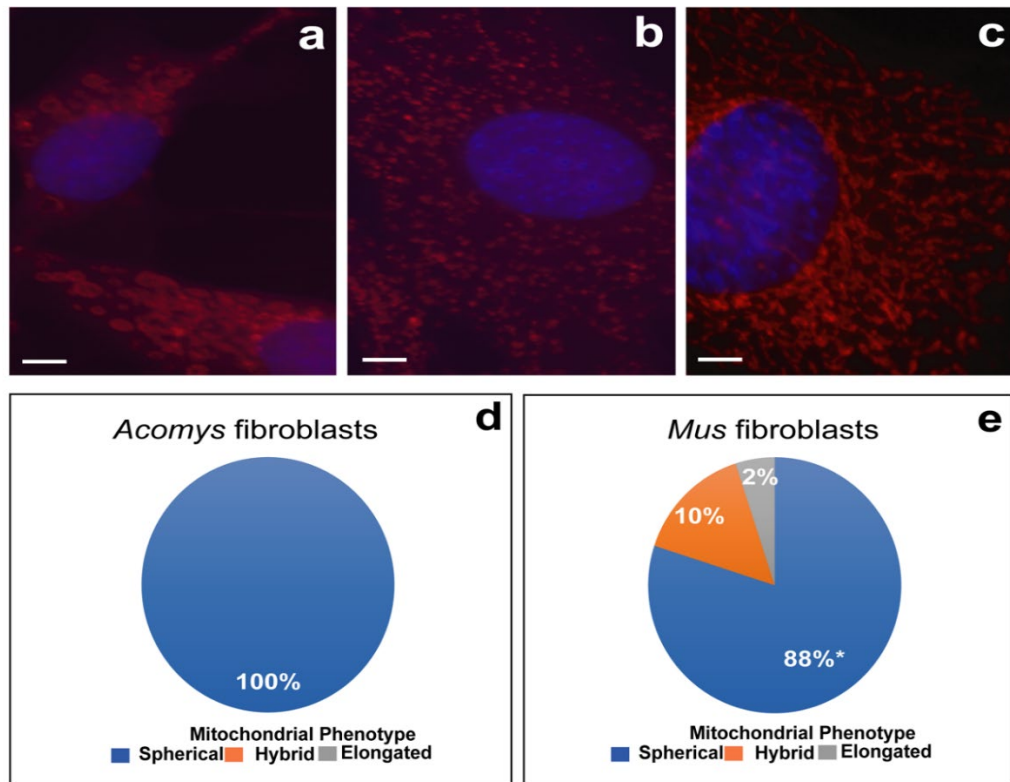


Figure 5. Mitochondria from *Acomys* and *Mus* fibroblasts differ phenotypically and functionally.

Acomys fibroblasts show a prominently dominant spherical mitochondrial phenotype (a). *Mus* fibroblasts have elongated and hybrid mitochondrial phenotypes (c) and also exhibit spherical mitochondria, although small (b). Scale bars: 5 μ m.

3.1.3 Mitochondria isolated from *Acomys* and *Mus* fibroblasts differ in membrane potential levels

To specifically quantify membrane potential independent of mitochondrial number and mass, we isolated mitochondria from primary fibroblasts and used a TMRE assay. We

used oligomycin and FCCP to maximally depolarize and re-polarize the inner mitochondrial membrane. While the membrane potential of *Mus* mitochondria trended higher compared to *Acomys* it was not significant ($n=3/\text{species}$, $P=0.0956$). It was expected that this difference would be more distinct due to their basal ECAR and OCR differences and may be addressed by increasing the sample size.

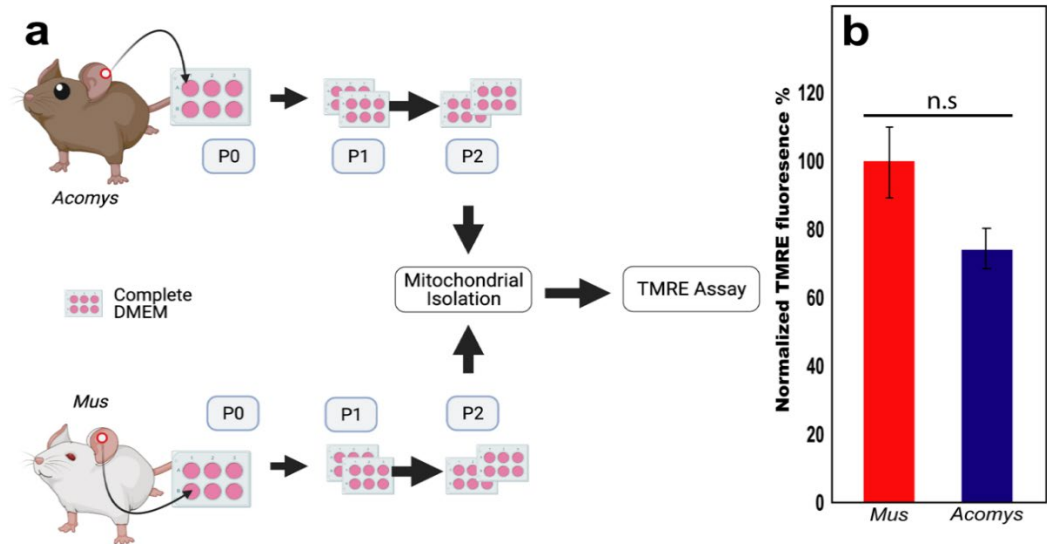


Figure 6. Mitochondria membrane potential in *Mus* fibroblasts trend higher compared to *Acomys*

Primary ear pinna fibroblasts were isolated from *Acomys* and *Mus*, cultured in complete DMEM, and pooled after two passages. Mitochondria were isolated from the pooled cells(a). TMRE analysis (b) shows higher ($P=0.0956$) membrane potential level trend in mitochondria isolated from *Mus* fibroblasts compared to that of *Acomys*. Scale bars: 5 μm . Error bars= \pm S.E.M. Created with BioRender.com

3.2 Substrate starvation tests.

A previous report from our lab showed that fibroblasts from *Acomys* and *Oryctolagus*, two mammals that possess enhanced regenerative ability, demonstrated unusually oxygen consumption rates (Saxena et al., 2019). In a bid to determine if there were different aspects of metabolism in fibroblasts isolated from regenerating mammals which differed significantly from those in non-regenerators, substrate starvation experiments were designed and carried out with fibroblasts isolated from ear tissue biopsies. With *Acomys* fibroblasts already characterized as having comparatively low OxPHOS rates and concurrent fetal/stem cell-like mitochondrial phenotypes (unpublished), we hypothesized that fibroblasts from regenerative species would possess a shift towards glycolysis-dependent metabolic phenotypes as seen in highly proliferative cancer cells (Warburg, 1956). Ear pinna fibroblasts were cultured in two conditions: 1) complete DMEM and 2) glucose deprived DMEM for two passages. The cells were then seeded into a Seahorse Assay plate and assayed for glycolytic flux, and oxidative phosphorylation under the two

conditions. The P2 cells were also stained using the Mitotracker red stain to determine any structural changes in mitochondrial phenotype in response to glucose starvation between both species.

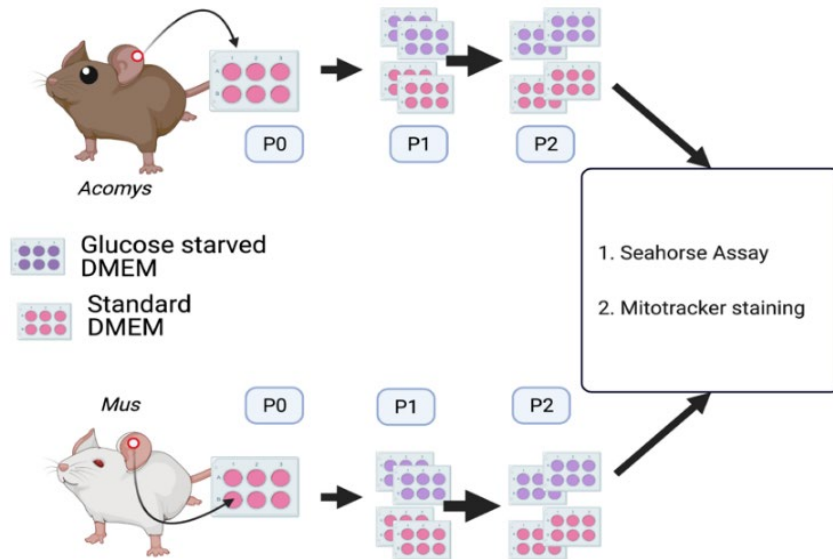


Figure 7. Schematic for glucose starvation experiments.

Fibroblasts were cultured in complete DMEM and glucose deficient DMEM for two passages, after which Seahorse Assay and Mitotracker red staining was carried out. Created with BioRender.com

3.2.1 Mitochondria from *Acomys* fibroblasts undergo substantial structural changes in response to glucose starvation, while *Mus* mitochondria change minimally in response to glucose starvation.

It is generally understood that elongated mitochondria exhibit more efficient oxidative phosphorylation due to a larger membrane surface area (Gomes, Di Benedetto, & Scorrano, 2011). Unpublished work from our lab reports that fibroblasts from non-regenerating species have higher mitochondrial mass/cell compared to fibroblasts from regenerating mammals. We hypothesized that removing glucose would force a physiological change that would be reflected in mitochondrial phenotype. For these experiments, four mitochondrial phenotypes were used for classifying Mitotracker-stained fibroblasts from both species: spherical (round and in some cases, massive), minimally hybrid (cells with a spherical: elongated mitochondrial phenotype ratio between 50% to 80%), prominently hybrid (cells with a spherical: elongated mitochondrial phenotype ratio between 30% to 50%) and elongated (Figure 7a-d). We found that in response to chronic glucose starvation, *Acomys* mitochondria shifted phenotype away from primarily spherical mitochondria ($63 \pm 3.3\%$ of cells) towards a prominently hybrid phenotype ($35 \pm 15\%$ of cells) (Figure 7e-f) with the portion of cells with elongated mitochondria doubling from $7 \pm 1.6\%$ to $15 \pm 5.7\%$. In contrast to the significant shift observed in *Acomys* fibroblasts

following glucose starvation, we observed only a slight, 2% and 5% increase, respectively in the elongated and prominently hybrid phenotype in *Mus* (Figure 10e-f). These data support a greater reliance on glucose to support basal metabolism in *Acomys* compared to *Mus* fibroblasts.

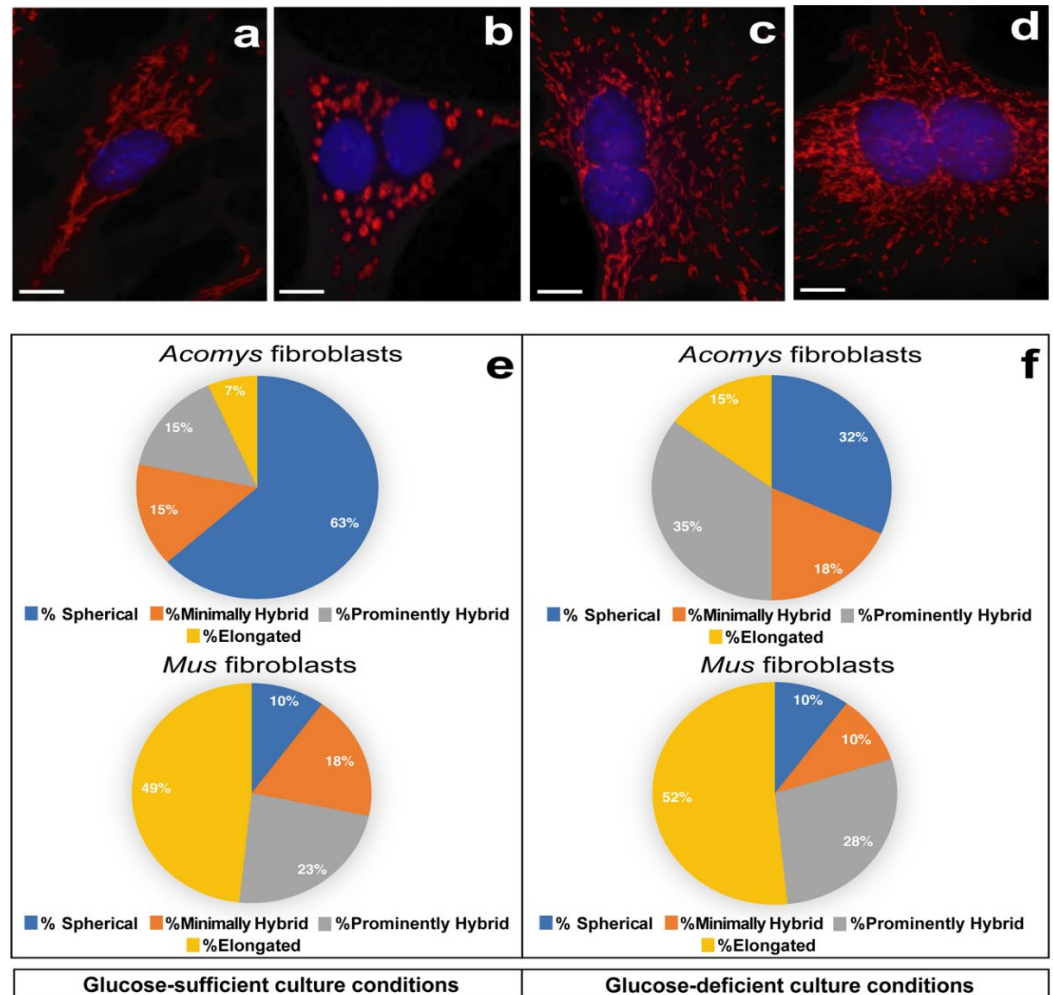


Figure 8. Mitochondria from *Acomys* and *Mus* fibroblasts differ in their phenotypic response to glucose deprivation.

Different mitochondrial features were used for classifying cells as having Elongated (a), Spherical (b), Minimally hybrid (c) and Prominently hybrid (d). Representations of glucose starved *Acomys* (e) and *Mus* fibroblasts mitochondrial phenotypes(f). Classification was carried out manually. Scale bars: 10 μ m.

3.2.2 *Acomys* fibroblasts do not show a significant metabolic response to glucose deprivation despite changes in mitochondrial phenotype.

In response to glucose starvation, *Acomys* fibroblasts did not show a significant change in OCR measures, ($P_{BR}= 0.5282$, $P_{MR}= 0.1346$, $P_{ATP}= 0.2036$), with the exception of proton leak ($P= 0.0240$), while in *Mus* fibroblasts, mitochondrial oxidative phosphorylation measures were significantly increased in response to glucose deprivation

(Figure 9a-d). Specifically, *Mus* fibroblasts showed a significant increase in Basal respiration (ANOVA, $F= 13.5979$, $n=3/\text{species}$, $P= 0.006$, 95% CI: 3.99 to 18.96), maximal respiration (ANOVA, $F= 13.9501$, $P < 0.0001$, 95% CI: 23.63 to 50.84), ATP-linked respiration (ANOVA, $F= 21.2104$, $P = 0.007$, 95% CI: 1.75 to 8.93) and proton leak (ANOVA, $F= 12.5663$, $P < 0.0001$, 95% CI: 1.49 to 3.10) (Figure 9a-d). For all comparisons, measured OCR was converted to percent normalized OCR. Contrary to our expectations, even though the *Acomys* fibroblast mitochondria seemed to shift more towards a tubular-esque phenotype, this did not match the corresponding OCR levels in *Acomys* fibroblasts, possibly suggesting that the mitochondrial structural change observed in *Acomys* served as a compensatory mechanism. In *Mus* fibroblasts however, the increased OCR levels in response to glucose deprivation may be attributed to the absence of a similar compensatory mechanism.

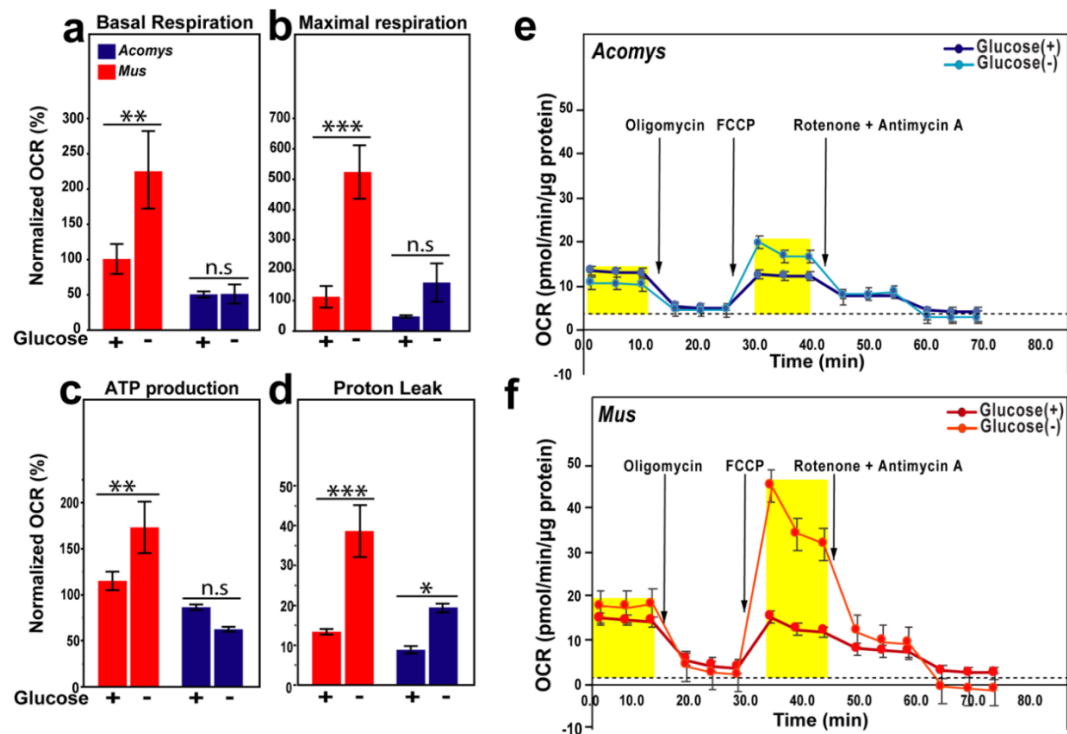


Figure 9. *Acomys* fibroblasts resist glucose starvation-induced increases in oxidative phosphorylation.

Mus fibroblasts showed significant increases in Basal respiration (a), Maximal respiration (b), ATP-linked respiration (c), and Proton leak (d). With the exception of Proton leak, changes in Basal respiration, Maximal respiration, and ATP measures in *Acomys* after glucose starvation was insignificant. Time course from mitochondrial stress testing conducted on an XF94 analyzer on (e) *Acomys* and (f) *Mus* fibroblasts after culturing in glucose sufficient and glucose deficient conditions. $n=3/\text{species}$. Mitochondrial inhibitors: Oligomycin, FCCP, Rotenone and Antimycin A were used to calculate different OXPHOS parameters(a), (b), (c) and (d). FCCP: Carbonyl cyanide-p-trifluoromethoxy phenyl hydrazine. Measured OCR was converted to percent normalized OCR. Error bars= \pm S.E.M.

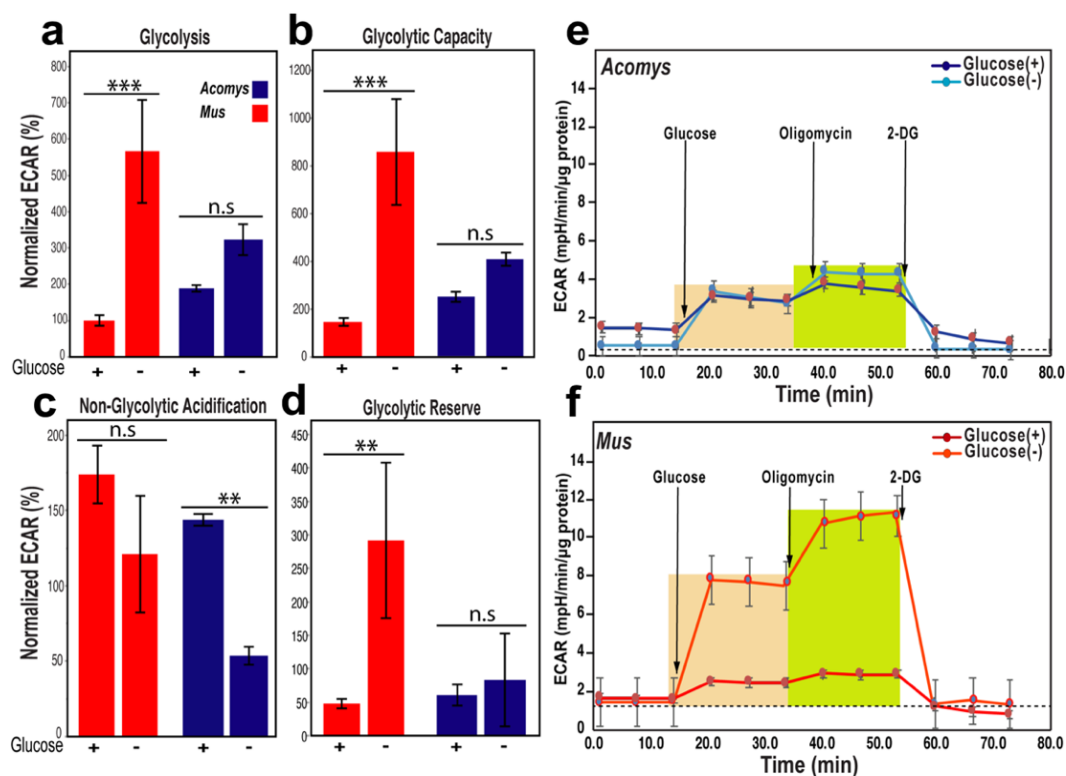


Figure 10. *Acomys* fibroblasts resist glucose starvation-induced increases in glycolytic flux. *Mus* fibroblasts showed significant increases in glycolysis (a), glycolytic capacity (b), and glycolytic reserve (c), with no significant change in Non-glycolytic acidification (d). In detail, in response to glucose deprivation, *Mus* fibroblasts showed significant increase in glycolysis (ANOVA, $F= 16.2488$, $n=3/\text{species}$, $P = 0.0002$, 95% CI: 2.56 to 6.02), glycolytic capacity (ANOVA, $F= 14.9475$, $P = 0.0001$, 95% CI: 3.94 to 9.15), and glycolytic reserve (ANOVA, $F= 3.8995$, $P = 0.0089$; 95% CI: 0.68 to 3.84). With the exception of non-glycolytic acidification, changes in glycolysis, glycolytic capacity, and glycolytic reserve measures in *Acomys* after glucose starvation were insignificant ($P_{\text{Glycolysis}} = 0.1444$, $P_{\text{Glycolytic Capacity}} = 0.2488$, $P_{\text{Glycolytic Reserve}} = 0.7702$). Time course from glycolytic stress testing conducted on an XF94 analyzer on (e) *Acomys* and (f) *Mus* fibroblasts after culturing in glucose sufficient and glucose deficient conditions. $n=3/\text{species}$. Glucose, Oligomycin, and 2-DG were used to calculate different glycolytic parameters (a), (b), (c) and (d). 2-DG = 2-deoxy-glucose. Measured ECAR was converted to percent normalized ECAR. Error bars = \pm S.E.M.

3.2.3 *Acomys* fibroblasts do not show significant changes in glycolytic response following glucose administration to glucose starved cells.

In light of our data showing that *Acomys* fibroblasts did not respond metabolically to glucose starvation, we next performed a glycolytic stress test under normal conditions and in response to glucose starvation (Figure 10). When glucose was added to *Mus* fibroblasts that had been deprived for two passages, glycolytic flux parameters increased significantly (Figure 10). The only ECAR parameter which showed no significant change in response to glucose deprivation in *Mus* fibroblasts, was non-glycolytic acidification ($n=3/\text{species}$, $P = 0.0763$). Conversely when *Acomys* fibroblasts deprived of glucose

suddenly experienced excess glucose, the ECAR parameters were not altered significantly with the exception of non-glycolytic acidification ($P = 0.0062$). Together, with our OxPHOS measurements in response to glucose starvation, these results demonstrate that *Acomys* fibroblasts, unlike the *Mus* fibroblasts, do not significantly increase metabolic parameters in response to glucose starvation. These results suggest that *Acomys* fibroblasts may be adapting to utilize an alternate fuel source. It is also key to note that *Acomys* and *Mus* fibroblasts, maintained their proliferative rates in either condition (not shown).

3.3 Glutamine metabolism inhibition experiments (within the scope of glucose deprivation).

Our Seahorse experiments analyzing OxPHOS and glycolysis in normal and glucose deprived media suggested *Acomys* fibroblasts were not acutely or chronically dependent on OxPHOS and glycolysis to meet their normal energy demands. We reasoned that *Acomys* may be maximally utilizing glutamine for accounting for the glucose-deprived decrease in mitochondrial oxidative phosphorylation (Pinkus, 1977). Since glutamine is a key anaplerotic metabolic substrate for the Krebs cycle, we next asked whether it might be the major source of metabolic fuel for *Acomys* fibroblasts. Previous work from our lab showed that in the face of ROS exposure, *Acomys* fibroblasts rapidly increased GPx antioxidant activity compared to *Mus* fibroblasts (Saxena et al., 2019). This result raised three possibilities: 1) higher GPx expression with standard Glutamine metabolism, 2) standard GPx expression with significantly pronounced glutamine metabolism, or 3) both. To distinguish these possibilities, fibroblasts from both species were cultured in complete DMEM and glucose deficient DMEM and seeded into Seahorse culture plates as described earlier. Four hours before the cells were run through the Seahorse analyzer, they were treated with 10 μ M BPTES. Both control media and BPTES media contained DMSO as this was used as a solvent for BPTES (0.1% v/v DMSO/DMEM in both conditions) (Figure 11). BPTES inhibits GLS, an enzyme which converts glutamine to glutamate (Tsai et al., 2020). This enzyme plays a central role in glutamine metabolism as its end product contributes anaplerotically towards the TCA cycle, and purine and pyrimidine synthesis.

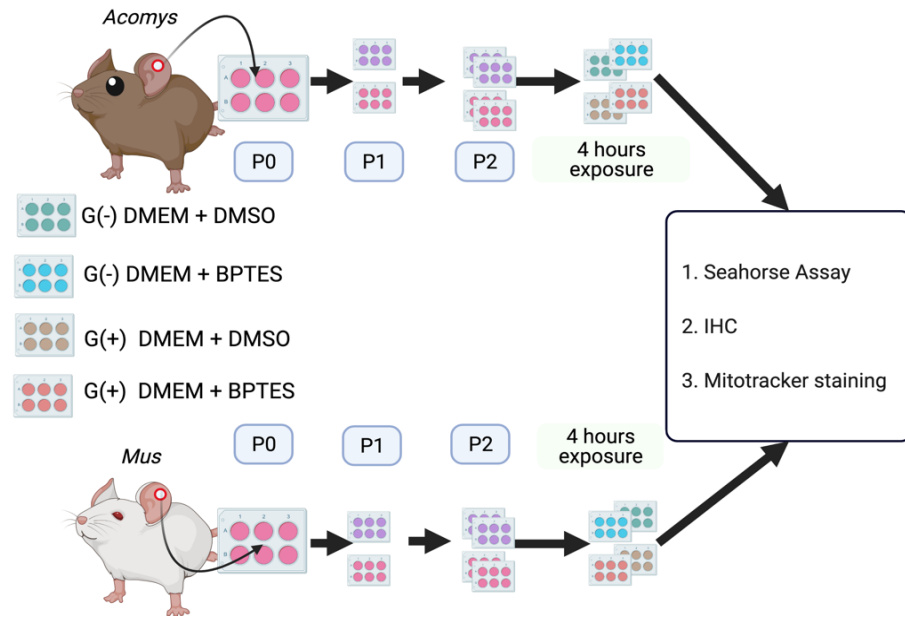


Figure 11. Schematic for glutamine metabolism inhibition experiments.

After isolation from ear punch biopsies, cells from both species were culture in complete and glucose deficient DMEM for two passages. 4 hours before Seahorse, immunocytochemistry, and Mitotracker staining, the cells in their respective conditions were treated with either BPTES (10 μ) or DMSO (0.1%). Created with BioRender.com

3.3.1 Within-specie comparisons of OCR parameters in response to BPTES treatment.

Next, we analyzed OCR in response to BPTES treatment where glucose was not limiting. When we analyzed OCR parameters from *Acomys* fibroblasts cultured in complete DMEM (with DMSO) and with BPTES in complete DMEM, we did not find a significant difference in basal respiration, maximal respiration, or ATP-linked levels ($P_{BR\ Acomys} = 0.998$; $P_{MR\ Acomys} = 0.3713$; $P_{ATP\ Acomys} = 0.2027$). DMSO-exposed *Mus* fibroblasts cultured in glucose-deficient DMEM had significantly higher levels of Maximal respiration compared to DMSO-exposed *Mus* fibroblasts grown in complete DMEM (ANOVA_{Treatment*Conditions*Species}, $F = 17.8573$, $MD_{Mus} = -443.7$, $P_{Mus} < 0.0001$, 95% CI_{Mus} : -662.1 to -225.4), BPTES-treated *Mus* fibroblasts cultured in complete DMEM ($MD_{Mus} = -572.8$, $P_{Mus} < 0.0001$, 95% CI_{Mus} : -768.0 to -377.5), and BPTES-treated glucose-starved *Mus* fibroblasts ($MD_{Mus} = -549.9$, $P_{Mus} < 0.0001$, 95% CI_{Mus} : -745.2 to -354.6) (Figure 9).

Since my earlier experiments indicated intrinsic differences in OCR response parameters to glucose starvation, it was necessary to determine the contributory role of glutamine α -ketoglutarate to mitochondrial respiration in the absence of glucose. Thus, we next monitored OCR parameters in response to BPTES treatment with and without glucose availability. Among all the OCR parameters, we observed no significant differences in

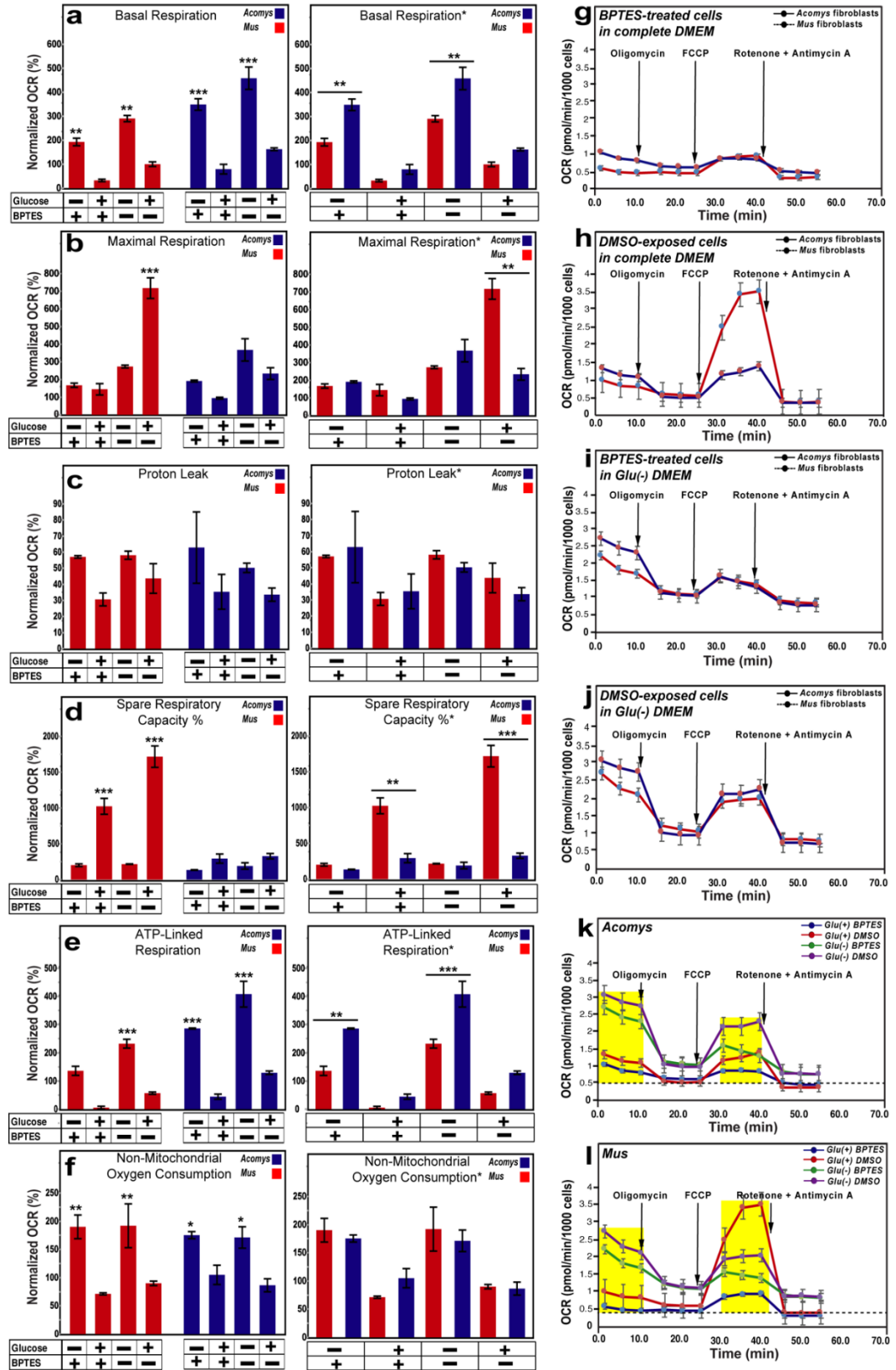


Figure 12. Glutamine metabolism inhibition in the light of glucose availability elicits different responses in mitochondrial respiration in *Acomys* and *Mus* fibroblasts.

Within-and-between-species OCR parameters namely Basal respiration (a), Maximal respiration (b), Proton leak (c), Spare respiratory capacity % (d) ATP-linked respiration (e) and Non-Mitochondrial Oxygen consumption (f) measured in *Acomys* and *Mus* fibroblasts after DMSO and BPTES exposure in glucose deficient and glucose sufficient conditions. Time course from mitochondrial stress testing conducted on an XF94 analyzer on *Acomys* and *Mus* fibroblasts under different conditions; BPTES-treated cells cultured in complete DMEM (g), DMSO-exposed cells cultured in complete DMEM (h), BPTES-treated cells cultured in glucose deprived DMEM (i), and DMSO-exposed cells cultured in glucose-deficient DMEM (j). n=3/species. OCR Time course summaries for all conditions were indicated in *Acomys* (k) and *Mus* (l) fibroblasts respectively. Mitochondrial inhibitors: Oligomycin FCCP, Rotenone and Antimycin A were used to calculate different OXPHOS parameters (a-f) FCCP: Carbonyl cyanide-p-trifluoromethoxy phenyl hydrazone. Measured OCR was converted to percent normalized OCR. Error bars= \pm S.E.M.

either species between BPTES treated media and control media (DMSO+DMEM) that were glucose-deficient: basal respiration (ANOVA_{Treatment*Species.BR}, $F= 0.1736$, $P_{Acomys} = 0.0864$, $P_{Mus} = 0.1534$), maximal respiration (ANOVA_{Treatment*Species.MR} $F= 9.2849$, $P_{Acomys} = 0.1536$, $P_{Mus} = 0.6672$), spare respiratory capacity (ANOVA_{Treatment*Species.SRC} $F= 23.4045$, $P_{Acomys} = 0.9970$, $P_{Mus} = 1.0000$), proton leak (ANOVA_{Treatment*Species.PL} $F= 1.6652$, $P_{Acomys} = 0.9421$, $P_{Mus} = 1.0000$) and non-mitochondrial oxygen consumption (ANOVA_{Treatment*Species.NMOC} $F= 0.8169$, $P_{Acomys} = 1.0000$, $P_{Mus} = 1.0000$) (Figure 9). The one exception we observed was for ATP linked respiration, where in both species, BPTES treatment significantly reduced glucose starved cells OCR levels ($P_{Acomys} = 0.0283$, 95% CI $Acomys$: -233.9 to -10.4, $P_{Mus} < 0.0001$, 95% CI Mus : -372.3 to -172.4). Basal respiration observations showed increased OCR recorded in glucose-starved fibroblasts in both species when compared to their respective controls (ANOVA_{Conditions} $F= 193.8446$, $P_{Acomys} < 0.0001$, 95% CI $Acomys$: 188.2 to 403.8, $P_{Mus} = 0.0015$, 95% CI Mus : 69.8 to 310.8). Proton leak measurements were negligible between different conditions and treatments in both species (Figure 9). Here, we observe that *Mus* fibroblasts mirror the effects of glucose deprivation with respect to oxygen consumption, whereas *Acomys* fibroblasts show significant increases in oxygen consumption in response to glucose removal contrary to what was observed in the substrate starvation experiments. In both species, BPTES treatment noticeably reduced oxygen consumption regardless of glucose availability.

3.3.2 Across-specie comparisons of OCR parameters in response to BPTES treatment

Interestingly, proton leak measurements between *Acomys* and *Mus* fibroblasts in all conditions didn't show any significant differences (ANOVA_{Treatment*Conditions*Species}, $F= 0.0028$, $P_{Complete\ DMEM + BPTES} = 0.9998$; $P_{Complete\ DMEM + DMSO} = 0.9670$; $P_{G(-)\ DMEM + BPTES} = 0.9993$; $P_{G(-)\ DMEM + DMSO} = 0.9958$) (Figure 9). Among DMSO-exposed fibroblasts cultured in complete DMEM, maximal respiration levels were significantly lower in *Acomys* than in *Mus* (ANOVA_{Conditions*Species}, $F= 29.8833$, $P_{Acomys} < 0.0001$, 95% CI $Acomys$: -678.9 to -288.4). This mirrored what was observed in previous experiments and was reflected in the

spare respiratory capacity observations as well (ANOVA_{Conditions*Species}, $F= 59.9915$, $P_{Acomys} < 0.0001$, 95% CI $Acomys$: -688.1 to -403.8)

In glucose-deficient conditions, basal respiration and ATP-linked respiration OCRs recorded were remarkably higher in *Acomys* than in *Mus* (ANOVA_{Species*Conditions.BR}, $F= 10.6591$, $P_{BR\ Acomys} = 0.0045$, 95% CI $BR\ Acomys$ =47.5 to 288.5; ANOVA_{Species*Conditions.ATP}, $F= 12.3664$, $P_{ATP\ Acomys} = 0.0018$, 95% CI $ATP\ Acomys$ =64.1 to 287.6), quite contrary to what was observed in the initial glucose starvation experiments where both parameters remained significantly unchanged in *Acomys* fibroblasts (and lesser to that observed in *Mus* fibroblasts) in response to glucose starvation (Figure 5). BPTES treatment is unlikely to be the factor behind this spike in *Acomys* fibroblasts basal respiration levels, as there was no significant difference in basal respiration levels between glucose starved *Acomys* fibroblasts that were BPTES treated and those exposed to DMSO ($P_{Acomys} = 0.0864$). BPTES rather caused a decrease in ATP-linked respiration (ANOVA_{Treatment}, $F= 33.8368$, MD $Acomys$ =-112.1, $P_{Acomys} = 0.0283$, 95% CI $Acomys$: -233.9 to -10.4) among glucose-starved *Acomys* fibroblasts (Figure 9a-f).

Since DMSO was used as the solvent for the BPTES used, the most likely common factor that could possibly explain this sharp spike in *Acomys* fibroblasts would be the combined effect of glucose starvation and DMSO exposure. Since DMSO at low complications has been reported to exert its cytotoxicity metabolically through mitochondrial membrane potential impedance, mitochondrial bloating, and ROS production (C. Yuan et al., 2014), this together with glucose starvation-induced stress, may best explain this observation in *Acomys* fibroblasts. It is key to note that this pro-OxPHOS effect was more pronounced in *Acomys*.

3.3.3 Within-specie comparisons of ECAR parameters in response to BPTES treatment

In both species, glycolytic levels decreased significantly in response BPTES under conditions of glucose starvation ($P_{Acomys} = 0.0009$, 95% CI $Acomys$: 24.5 to 105.8; $P_{Mus} = 0.0019$, 95% CI Mus : 19.8 to 101.1). Also, there was a noticeable BPTES-induced decrease in glycolytic reserve levels in both species under conditions of glucose availability although these differences weren't significant ($P_{Acomys}=0.0766$; $P_{Mus}= 0.353$), which was unexpected, especially in *Acomys*.

Glycolytic capacity levels in both species were unaffected by BPTES exposure ($P_{Acomys}=0.141$; $P_{Mus}= 0.927$) but were increased significantly (ANOVA_{Conditions}, $F= 250.7790$, $P_{Acomys} < 0.0001$, 95% CI $Acomys$: 71.7 to 158.8; $P_{Mus} < 0.0001$, 95% CI Mus : 49.1 to 136.1) in response to glucose starvation (Figure 10b). This trend was observed in both species in glycolytic reserve (Figure 10c) measurements (ANOVA_{Conditions}, $F= 256.5742$, $P_{Acomys} < 0.0001$, 95% CI $Acomys$: 71.7 to 158.8; $P_{Mus} < 0.0001$, 95% CI Mus : 49.1 to 136.1). Non-glycolytic acidification levels in *Acomys* were unaffected by BPTES treatment nor glucose availability (Figure 10e), although in *Mus*, this effect was mediated by glucose starvation ($P_{Mus} < 0.0024$, 95% CI Mus : 5.4 to 28.5).

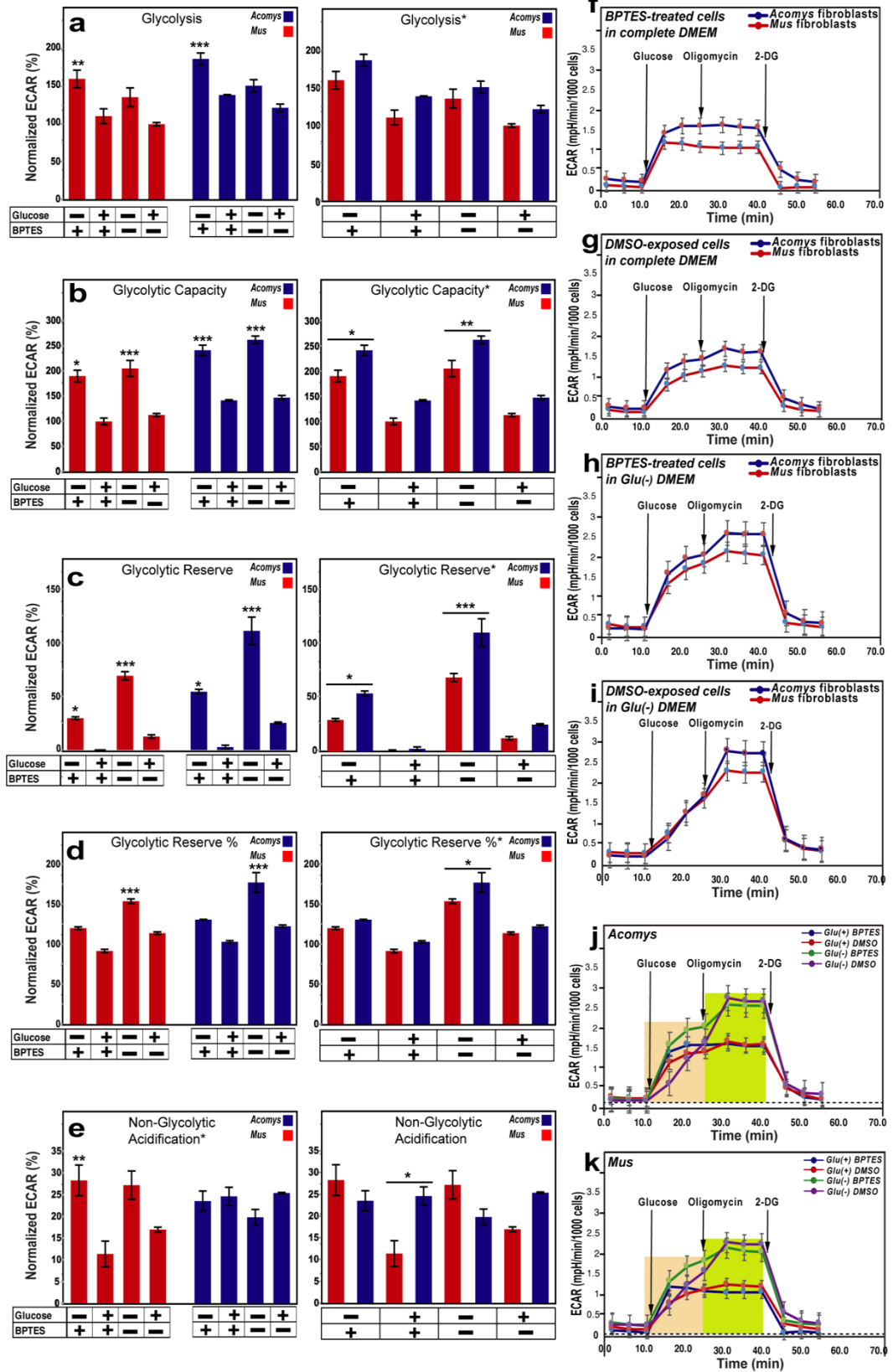


Figure 13. Glutamine metabolism inhibition in the light of glucose availability elicits different glycolytic responses in *Acomys* and *Mus* fibroblasts.

Within and between species ECAR parameters namely Glycolysis (a), glycolytic capacity (b), glycolytic reserve (c), glycolytic reserve% (d) and non-glycolytic acidification (e) measured in *Acomys* and *Mus* fibroblasts after DMSO and BPTES exposure in glucose deficient and glucose sufficient conditions. Time course from glycolytic stress testing conducted on an XF94 analyzer on *Acomys* and *Mus* fibroblasts under different conditions; BPTES-treated cells cultured in complete DMEM (f), DMSO-exposed cells cultured in complete DMEM (g), BPTES-treated cells cultured in glucose deprived DMEM (h), and DMSO-exposed cells cultured in glucose-deficient DMEM (h). ECAR Time course summaries for all conditions were indicated in *Acomys* (k) and *Mus* (l) fibroblasts respectively. n=3/species. Glucose, Oligomycin, and 2-DG were used to calculate different glycolytic parameters. 2-DG = 2-deoxy-glucose. Measured ECAR was converted to percent normalized ECAR. Error bars= \pm S.E.M.

3.3.4 Across-specie comparisons of ECAR parameters in response to BPTES treatment

Despite *Acomys* fibroblasts showing higher levels of glycolysis than *Mus* fibroblasts in every condition (Figure 13), none of these differences were significant, interestingly (ANOVA_{Treatment*Conditions*Species}, $F=0.0428$, $P_{\text{Complete DMEM} + \text{BPTES}}=0.3007$; $P_{\text{Complete DMEM} + \text{DMSO}}=0.5924$; $P_{G(-) \text{ DMEM} + \text{BPTES}}=0.3679$; $P_{G(-) \text{ DMEM} + \text{DMSO}}=0.8849$).

In glucose-starved conditions, whether with ($P_{\text{Acomys}}=0.0152$, 95% CI *Acomys*: 7.8 to 94.8) or without BPTES treatment ($P_{\text{Acomys}}=0.0061$, 95% CI *Acomys*: 13.7 to 100.7), *Acomys* fibroblasts showed significantly higher glycolytic capacity levels compared to *Mus* fibroblasts (Figure 10b). Under the same culture conditions, this trend was repeated in glycolytic reserve measurements (Figure 13c) between *Acomys* and *Mus* fibroblasts with ($P_{\text{Acomys}}=0.0428$, 95% CI *Acomys*: 0.6 to 48.9) and without BPTES treatment ($P_{\text{Acomys}}=0.0004$, 95% CI *Acomys*: 17.7 to 66.1). Only glucose-starved DMSO-exposed *Acomys* fibroblasts showed higher glycolytic reserve% levels than *Mus* fibroblasts in similar conditions (ANOVA_{Conditions}, $F=128.6312$, $P_{\text{Acomys}}=0.0449$, 95% CI *Acomys*: 0.4 to 46.4), the other conditions showed no significant across-specie differences in glycolytic reserve% levels ($P_{\text{Complete DMEM} + \text{BPTES}}=0.6683$; $P_{\text{Complete DMEM} + \text{DMSO}}=0.8916$; $P_{G(-) \text{ DMEM} + \text{BPTES}}=0.7358$). In conditions of glucose availability, non-glycolytic acidification levels were higher in *Acomys* than in *Mus*, with the differences significant with BPTES exposure (ANOVA_{Treatment*Conditions}, $F=25.2511$, $P_{\text{Acomys}}=0.0203$, 95% CI *Acomys*: 1.6 to 24.9) and insignificant without ($P_{\text{Acomys}}=0.2619$). In glucose-starved conditions, non-glycolytic acidification was lower in *Acomys* but insignificant with ($P_{\text{Acomys}}=0.8385$) and without BPTES treatment ($P_{\text{Acomys}}=0.4005$).

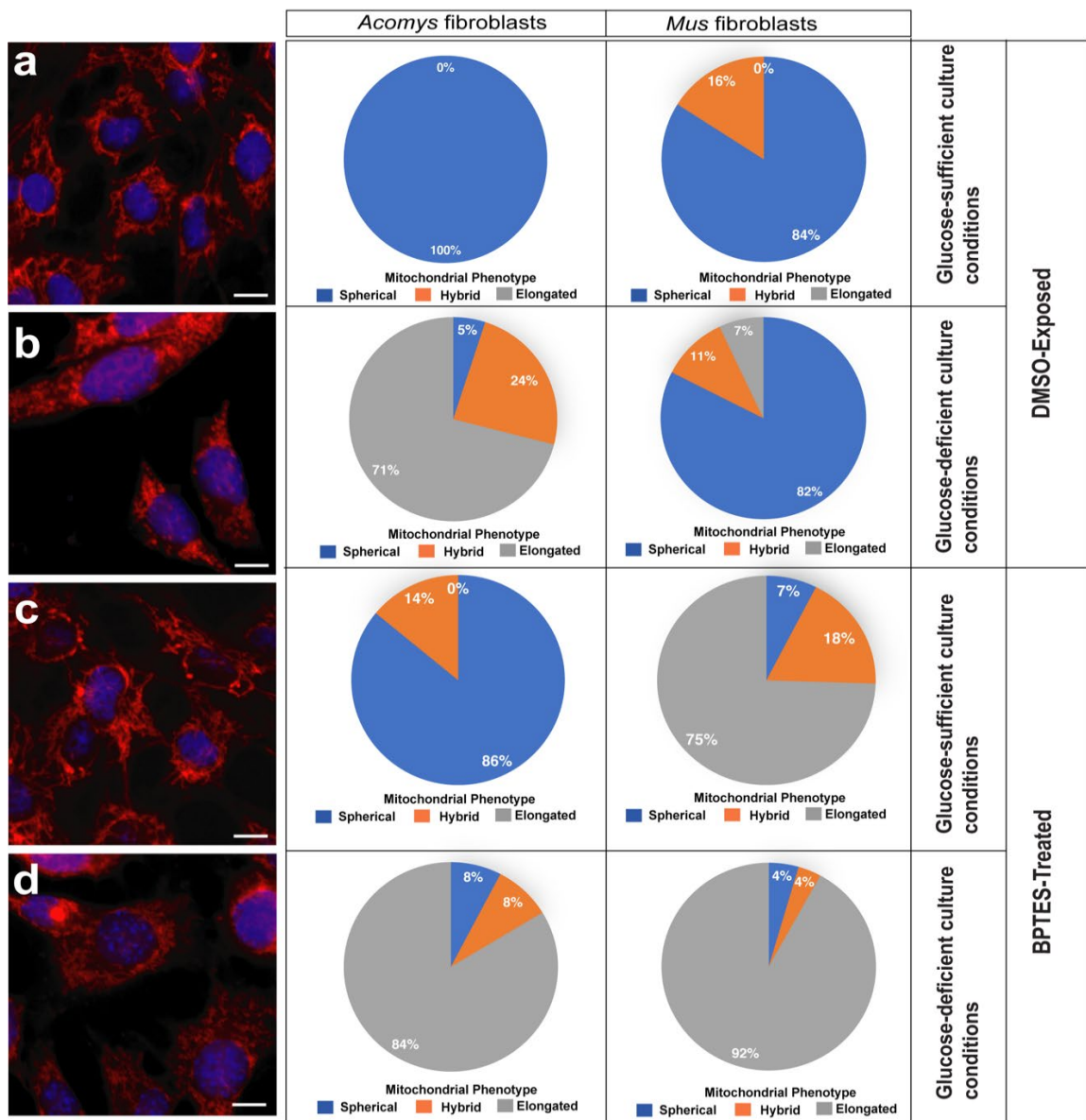


Figure 14. *Acomys* mitochondria dynamics are affected by glucose availability and DMSO exposure; BPTES treatment alters mitochondrial phenotype in *Mus* fibroblasts.

Different mitochondrial features were used for classifying cells as having Elongated, Spherical and Hybrid. Classification was carried out manually. *Acomys* fibroblasts show an elongated mitochondrial phenotype in response to glucose starvation (a: DMSO-exposed) and (c: BPTES-treated). *Mus* fibroblasts show an elongated mitochondrial phenotype in response to BPTES treatment (d) and retain the spherical phenotype when exposed to DMSO while glucose starved (b). Scale bars: 10 μ m.

3.3.5 *Acomys* fibroblasts mitochondria switch from a spherical to an elongated phenotype in response to glucose starvation and DMSO exposure.

BPTES treatment induced a transition from the prominently spherical phenotype (although with a visually lower mito:cell size ratio) to a prominently elongated phenotype in *Mus* fibroblasts under both glucose-deficient ($83 \pm 10.5\%$ spherical to $92 \pm 8\%$ elongated) and glucose-sufficient ($84 \pm 10.3\%$ spherical to $75 \pm 7.5\%$ elongated) conditions (Figure 14). This was a stark contrast to what was observed in *Acomys* fibroblasts, where BPTES treatment triggered a change to a prominently elongated phenotype under glucose deficient conditions (0% to $84 \pm 9.8\%$), while under glucose sufficient conditions there was an increase in the hybrid phenotype (0% to $14 \pm 8.4\%$), although the spherical phenotype was still dominant ($86 \pm 8.4\%$) (Figure 14). When compared to DMSO-exposure, we observe that the trend in mitochondrial shift to the elongated phenotype is consistent in *Acomys* under only under glucose-starved conditions, mirroring what was observed in response to BPTES treatment (Figure 14a,c). Even though BPTES and DMSO treatments were separate, it is key to observe that the common denominator was 0.1% DMSO as DMSO was used as a solvent. These results corroborate the OCR results observed with mitochondrial phenotype predicting physiological parameters in *Acomys*. What was puzzling however, was this seeming lack of correlation observed in *Mus* fibroblasts, which retained their prominently spherical mitochondrial phenotype ($84 \pm 10.3\%$ to $82 \pm 10.5\%$ spherical) under chronic glucose starvation conditions, when exposed to DMSO (Figure 14b,d). Together, we observe that *Acomys* mitochondrial phenotype supports the oxygen consumption levels measured in the Seahorse Assay, with glucose deprivation inducing significant mitochondrial respiration in both species. *Mus* mitochondria, however, are altered by BPTES treatment, although this is not mirrored in their corresponding respiration observations (Figure 12).

3.3.6 Glucose availability and BPTES treatment do not have an effect on *Acomys* fibroblast survivability.

Although not done in the previous glucose starvation experiments, it was incumbent to determine the combined effect of glucose starvation and glutamine metabolism inhibition on fibroblast proliferation and senescence in the light of DMSO exposure, and if they would correlate with the physiological parameters already observed. This is key, as the end product of GLS1 (inhibited by BPTES) is a precursor for glutathione production (antioxidant activity), α -ketoglutarate (TCA anaplerotic contribution), and proline-for collagen I synthesis (Hamanaka et al., 2019) and may have some off-target effects on cell survivability (Pinkus, 1977); (Murphy et al., 2018); (Tsai et al., 2020). Immunocytochemistry involving combined staining of DAPI, EdU and γ -H2AX was carried out on the fibroblasts cultured under conditions and treatments described above. BPTES treatment, and glucose availability exposure did not have effect (Figure 15) on senescence on *Acomys* fibroblasts ($P_{Complete\ DMEM + BPTES} = 0.9883$; $P_{G(-)\ DMEM + DMSO} = 0.9062$; $P_{G(-)\ DMEM + BPTES} = 0.8355$). In *Mus*, DMSO-exposed, glucose starved fibroblasts were more senescent than other fibroblasts cultured under other conditions

(ANOVA_{Treatment*Conditions*Species}, $F=18.6120$, $P_{Complete\ DMEM + BPTES}= 0.0331$; $P_{Complete\ DMEM + DMSO}=0.0035$; $P_{G(-)\ DMEM + BPTES}= 0.0002$). Put together, we report that although glucose deprivation induced (with DMSO exposure) increased mitochondrial respiration in both species, *Mus* fibroblasts exhibited increased senescence in response, whereas *Acomys* fibroblasts showed no increase in senescence regardless of glucose removal or BPTES treatment (Figure 15).

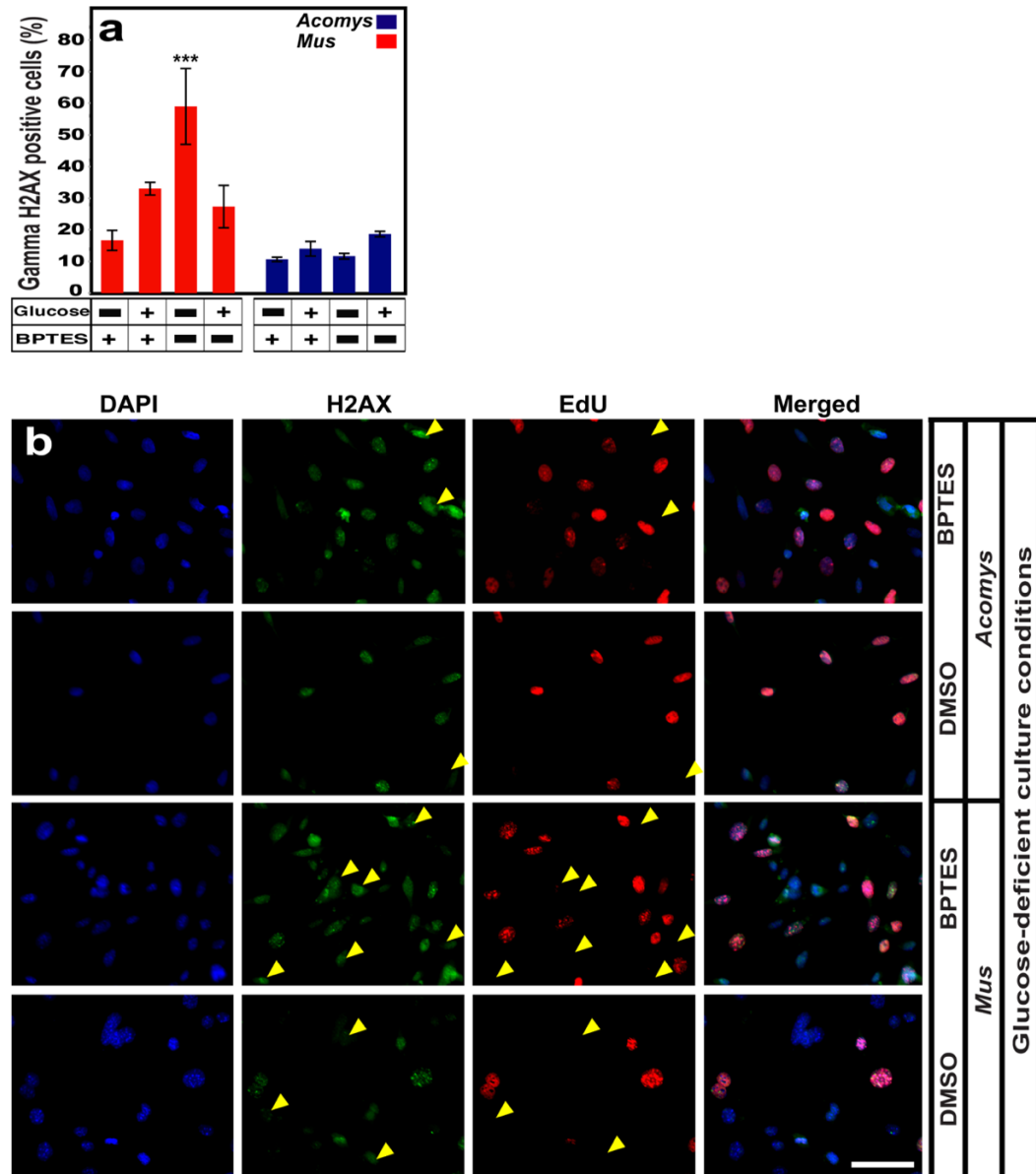


Figure 15. Glucose starvation and BPTES treatment do not have significant effect on cell survivability in *Acomys* fibroblasts. *Mus* fibroblast survivability drops under conditions of glucose starvation and DMSO exposure. Senescence was calculated by subtracting the number EdU-positive cells from γ -H2AX positive cells against the total number of cells (a). Yellow arrows indicate γ -H2AX positive cells which were not EdU positive. Scale bar: 25 μ m.

4. DISCUSSION

Compared to normal wounds, hypertrophic (keloid) and chronic wounds are populated with fibroblasts expressing unique transcriptomic signatures (Rinkevich et al., 2015), survival and signaling markers (Cook, Davies, Harding, & Thomas, 2000); (Wall et al., 2008); reviewed by (Huang, Murphy, Akaishi, & Ogawa, 2013). Given that fibroblast phenotype appears to correspond with specific pathological conditions, it is likely that cell autonomous features of cells within a wound environment in (wound contraction, lineage plasticity, ECM deposition and remodeling) can impact repair outcomes. Similarly, fibroblasts heterogeneity in fibroblast phenotype across different species may predict regenerative ability, with metabolic signatures acting as one potential source regulating different functional healing outcomes.

By quantifying oxygen consumption using a Seahorse analyzer and characterizing mitochondrial features in primary ear pinna fibroblasts from spiny mice (enhanced regenerative ability) and outbred laboratory mice (poorly regenerative), we observed that *Acomys* fibroblasts rely on glycolysis to support cellular metabolism and also possess a higher capacity for glycolysis compared to *Mus*. Conversely, *Mus* fibroblasts showed higher levels of basal respiration, maximal respiration, and spare respiratory capacity, findings that supported a hypothesis generated from previous work in our lab (Saxena et al., 2019). Building on these observations, we tested how fibroblasts from these species would respond to glucose starvation, which would allow us to test if glucose withdrawal would force *Acomys* fibroblasts to become more OxPHOS dependent. While *Mus* fibroblasts exhibited a significant increase in oxygen consumption and extracellular acidification rates after two passages in DMEM without glucose, *Acomys* fibroblasts appear unaffected and did not show a significant increase in either of these parameters. Although this data proved contradictory to our hypothesis, it suggested that *Acomys* fibroblasts might possess greater metabolic plasticity to maintain homeostasis compared to *Mus* fibroblasts.

To examine metabolic plasticity in greater depth we tested how fibroblasts from *Mus* and *Acomys* would behave when α -ketoglutarate uptake into the Krebs cycle was blocked using BPTES. BPTES treatment decreased oxygen consumption across all conditions in both species and this decrease was exacerbated when applied in combination with glucose starvation (Figure 12). We also observed the glycolytic contribution of glutamine when in both species BPTES treatment in the presence of glucose led to a dramatic drop in glycolytic capacity (almost 0% normalized ECAR). This supported reports of the involvement of glutamine in increasing or maintaining high levels of glycolytic ATP generation (Murphy et al., 2018). We also observed that glucose starvation caused significant increased OCR parameters in *Acomys* regardless of BPTES treatment. Further deliberation showed that DMSO (the BPTES solvent) caused this metabolic switch in *Acomys* under glucose deprived conditions corroborated by concomitant changes in mitochondrial phenotype (Figure 14). Just as observed in the mitochondrial stress tests, *Acomys* fibroblasts lost their glycolytic “plasticity” when glucose deprivation was combined with DMSO exposure (glycolysis, glycolytic capacity, glycolytic reserve), with

ECAR levels dropping in response to BPTES treatment only under glycolytic reserve parameters (Figure 13). Both ECAR and OCR results exhibit the anaplerotic contributions of glutamine to the TCA cycle and concurrently aerobic glycolytic function.

It is key to note that these sudden increases in OCR and ECAR in both species were being observed with the basis of determining the ability of the fibroblasts under study to utilize compensatory mechanisms to resist metabolic stress due to substrate manipulation *in vitro*. Keeping in mind that, although starvation conditions were maintained even during both mitochondrial and glycolytic stress tests, there was a window where glucose was introduced along with the injection of the different testing inhibitors and substrates, hence the results obtained have to be observed as cellular OCR and ECAR responses to glucose after prolonged starvation. Response time may not be used as the explanation for this phenomenon, as it was observed that *Acomys* fibroblasts maintained their OCR levels even in acute glucose starvation conditions (24 hours before testing: Supplemental Figure 1), indicating that this “plasticity” was independent of length of exposure. *Mus* fibroblasts on the other hand showed significant increase in OCR with response to time.

An organic solvent ideal for the dissolution of poorly soluble polar and non-polar solutes, DMSO is widely used in biomedical and pharmaceutical research due to its amphipathic nature. Due to its broad use, its effect on cellular processes has been classified as negligible at concentrations below 10% v/v. (Sumida et al., 2011); (Y. Yuan et al., 2016). DMSO’s cytotoxicity is reported to be mediated through pore formation in cellular plasma membranes. However, other reports have indicated that even below 10%, there are still some cytotoxic effects (Galvao et al., 2014); (Verheijen et al., 2019). With reference to cellular metabolism, some of the effects of DMSO exposure include increased ROS production, mitochondrial membrane potential debilitation, and mitochondrial swelling, which results in cytochrome c release in doses as low as 1% *in vitro* (C. Yuan et al., 2014). It has been recommended (Galvao et al., 2014) that in biomedical studies that require such solvents, other analogs of DMSO should be considered, options which are less cytotoxic, like ones developed and described by (Li et al., 2017). The alternative option, in conditions where analogs are unavailable, would be to factor in a third absolute control in such studies, in addition to treatment and solvent exposure, to be able to accurately ascertain the impact of DMSO exposure on the cultured cells independent of the dissolved treatment compound. In future experiments which would be set up to determine the direct influence of glucose and glutamine on differential levels reticence in response to ROS-induced senescence between regenerating on non-regenerating fibroblasts, these recommendations would be factored into experimental design.

Off-target effects of DMSO on cellular processes were expected, but these effects were most pronounced in *Acomys* fibroblasts. Previous reports from our lab (unpublished) have shown that fibroblasts from non-regenerators have higher mitochondrial mass compared to regenerators. This may explain this DMSO effect observed in *Acomys*. The TMRE assay run on mitochondria isolated from *Acomys* and *Mus* fibroblasts showed that when matched for mass, *Mus* mitochondria had higher membrane potential (although the

difference was not statistically significant, Figure 6), underlying an intrinsically more productive system for utilizing reducing equivalents for ATP synthesis. This may be due to differences in mitochondrial phenotype between the two species, keeping in mind that even when spherical mitochondria are observed in *Mus* fibroblasts, these mitochondria had noticeably smaller mito: cell or mito: nucleus ratios compared to *Acomys* which are massive and “doughnut-like”. This lower membrane potential observed in *Acomys* mitochondria may bely an intrinsically low-performing O_xPHOS-mediated ATP generation system, favoring a higher glycolytic flux. This bias towards glycolysis may explain the metabolic flexibility observed in *Acomys* fibroblasts in response to glucose starvation.

Nutrient starvation has been previously reported to have a role in mitochondrial dynamics: one study determined that a cAMP-PKA-mediated blocking mechanism of mitochondrial fission (DRP1) led to unopposed mitochondrial fusion resulting in mitochondrial elongation: a self-preservatory process protecting the mitochondria from starvation-induced autophagy (Gomes et al., 2011). As stated earlier, elongated mitochondria ramp up cristae biogenesis which in turn increases ATP synthase activity. Here, we report that even though there is a noticeable change in mitochondrial phenotype from the predominantly spherical to a hybrid one in response to glucose deficiency, *Acomys* fibroblasts resist a starvation-induced switch to a significant increase in Oxidative phosphorylation. We also report that by stroke of serendipity, this resistance to starvation-induced increase in O_xPHOS with a concurrent switch from the spherical to prominently elongated phenotype, is bypassed with the combined action of DMSO exposure and glucose starvation. Although this effect did not culminate in an increase in senescence, as assayed by γ H2AX phosphorylation (Figure 15), which may belie other possible compensatory mechanisms aside glutathione peroxidase (such as catalase), it is prudent to determine the role of this combined effect on *Acomys* fibroblasts metabolism and the associated mechanisms in its oxidative stress pathways.

Acomys fibroblasts seem to exhibit some mitochondrial/oxidative stress pathways which can be considered as “stem-like”, or better still, juvenile. With reports of high reticence to ROS, and passage number-induced senescence (Saxena et al., 2019) in addition to results reported here, *Acomys* fibroblasts seem to have intrinsic features (senescence-related mitochondrial/oxidative stress pathway signatures) which make them different from the average quiescent differentiated cell (Prigione et al., 2010). Aside its cytotoxic properties, DMSO has also been reported as responsible for significantly increasing pluripotent stem cell differentiation efficiency *in vitro* (Chetty et al., 2013). Even though we accept it is quite a stretch, our results suggest that glucose starvation and DMSO treatment may have uncovered the intrinsically “stem-like” properties of *Acomys* fibroblasts with the treatment causing as switch to a more “differentiated” metabolic phenotype. Current work is ongoing in the lab to ascertain differences in lineage plasticity between *Acomys* and *Mus* *in vitro*, and the inclusion of DMSO and glucose starvation in such experiments may throw more light on a possible dichotomy in the two species concerning this critical fibroblast function. There is also a need to repeat these experiments

in *Rattus* and *Oryctolagus* fibroblasts to determine if this response to DMSO and glucose starvation is dependent on proliferative ability (Saxena et al., 2019) or regeneration. Metabolically, we report that *Acomys* fibroblasts have higher antioxidant activity (Saxena et al., 2019), higher glycolytic flux, less mitochondria, are lower in OxPHOS rate, and show this “doughnut, spherical, fetal mitochondrial phenotype, even into old age (unpublished) compared to *Mus* fibroblasts.

Altogether, these results indicate that *Acomys* fibroblasts demonstrate a higher glycolytic bias *in vitro* compared to *Mus* fibroblasts which like typical differentiated cells, have higher OxPHOS rates (Figure 1) and that this glycolytic bias (coupled with associated mitochondrial properties) may play a pivotal role in conferring a homeostatically “plastic” state, with respect to glucose availability in *Acomys* fibroblasts. This metabolic plasticity, an intrinsic ability to resist metabolic state changes in response to glucose starvation, is lost when chronic glucose deprivation is coupled with 0.1 % DMSO exposure, uncovering a critical role for mitochondrial membrane integrity in the plasticity *Acomys* fibroblasts demonstrate. Despite the DMSO/glucose starvation-fueled switch to a high OxPHOS state, the expected rise in ROS-induced senescence is not seen in *Acomys* (Figure 15), suggesting a contribution from antioxidant mechanisms.

In addition to the results we obtained from the glucose and glutamine metabolism manipulation experiments, future directions should investigate the contribution of β -oxidation to the general metabolic state of regenerating and non-regenerating fibroblasts. β -oxidation of fatty acids produces acetyl coA for entry into the TCA cycle and generates NADPH as a by-product. In addition to its contribution towards nucleic acid and lipid synthesis, NADPH is a key contributor towards antioxidant function and is utilized by highly respiring cancer cells for mitigating high ROS levels (Choi et al., 2020). The possible contribution of glycogen metabolism (glycogenesis vs. glycogenolysis) and gluconeogenesis towards maintaining this plastic state in *Acomys* would have to be explored as well. With this in mind, carbon tracing metabolomic studies involving the “taking” of cytoplasmic “snapshots” of various metabolites and pathway intermediates would greatly inform on pathway flux efficiencies and bottlenecks, painting a broader but detailed picture about clear cut metabolic distinctions between fibroblasts from regenerators and non-regenerators. Transcriptomic analysis of the expression of important enzymes (GLUT2/ GLUT4, PDH, LDH, hexokinase) and enzyme regulators of the aforementioned pathways under basal conditions, as well as conditions of substrate deficiency would corroborate the data provided by metabolomic analysis.

The findings obtained from this study need to be interpreted in the light of the following significant limitations. Senescence detection in standard cultures (without DMSO or BPTES treatment) were not carried out, which would have provided a possible relationship between glucose starvation and the development of senescence in the two fibroblasts groups. In the glutamine metabolism inhibition experiments, two additional culturing conditions, namely complete DMEM and glucose starved DMEM, both without DMSO, would have accounted for the direct influence of DMSO on both sets of cell lines,

such that the effect of BPTES, the main treatment would be better appreciated. As shown in Figure 16, glutamine has pro-proliferation targets upstream of GLS1 which would be missed by BPTES treatment. Alternative inhibitors such as DON (6-Diazo-5-oxo-L-norleucine: an anticancer drug candidate) which inhibit glutamine metabolism upstream of GLS1 (Murphy et al., 2018) could be considered to determine differences in its broader effects between fibroblasts from regenerators and non-regenerators. Comments on compensatory antioxidant mechanisms in highly respiring *Acomys* fibroblasts would have to be validated by glutathione peroxidase assays to determine if BPTES-depleted glutamine has a direct effect on glutathione production, as alternate sources of glutamate could maintain Gpx activity. Manual characterization of mitochondrial phenotypes provides limited information and would need to be validated using particle detecting and characterizing software. Finally, discussions about ROS-protection in *Acomys* after the switch to a high OXPHOS state would need to be validated by a quantitative analysis of internally generated ROS in isolated mitochondria.

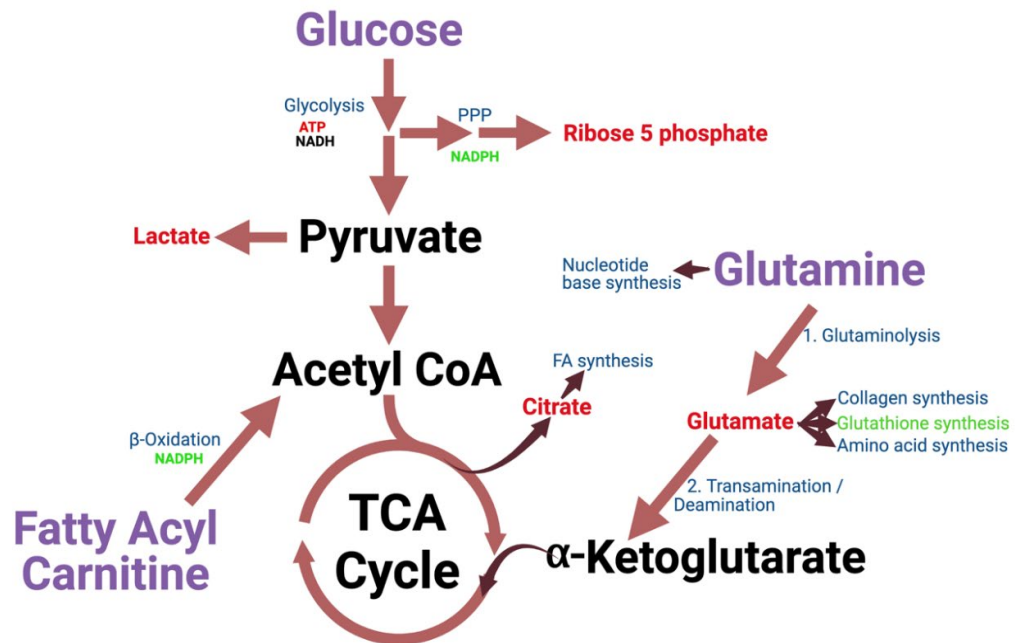
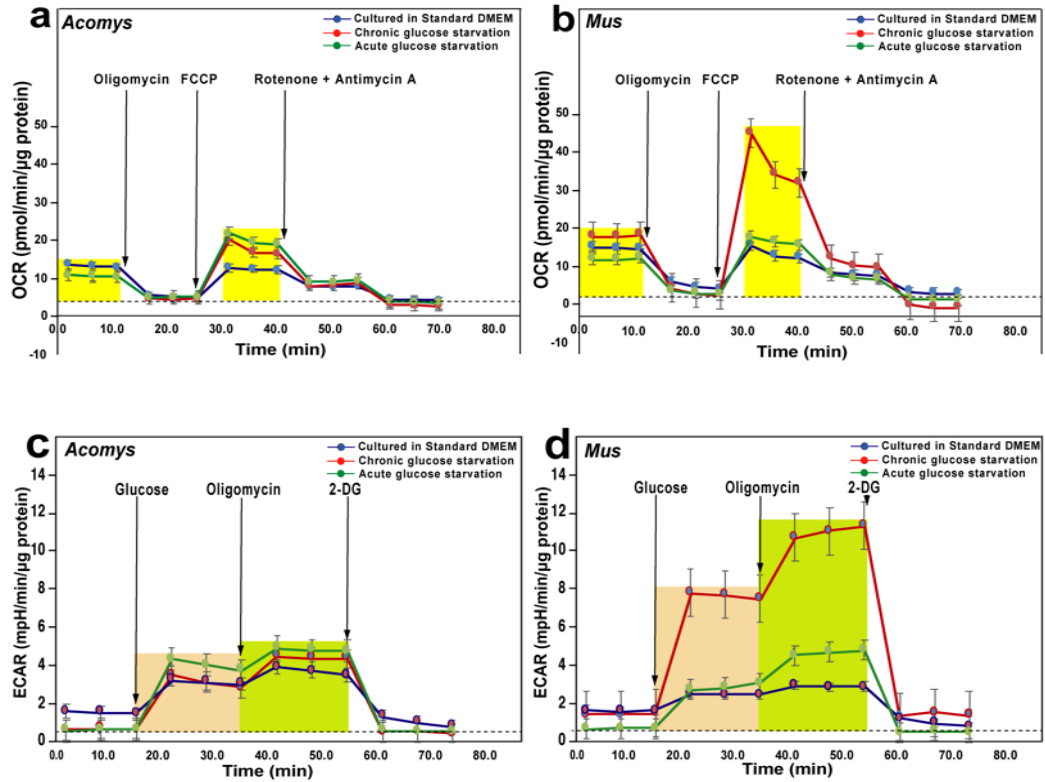


Figure 16. Key metabolic substrates produce and generate intermediates/products with anabolic, antioxidant and signaling functions

In this study, the differential contributions of Glucose and Glutamine in fibroblasts from regenerating and non-regenerating mammals have been assessed. Subsequent studies could focus on fatty acid oxidation and its associated antioxidant reducing equivalents. The use of inhibitors that target fatty acid synthesis, the pentose phosphate pathway, lactate synthesis and pyruvate oxidation could be instructive on differences in the movement of carbon *Acomys* and *Mus* fibroblasts. Created with BioRender.com

Further understanding of pro-regenerative metabolic signatures in tissue fibroblasts may serve as the foundation for predictive studies on regeneration, considering the recent push for the exploration of new models for biomedical research. This would allow for a simpler, broader, faster “litmus test” for regeneration on other non-traditional mammalian models, with its basis on the metabolic state of the tissue fibroblasts responsible for fibrotic or regenerative repair. With multiple reports on variant fibroblast sub-population phenotype forms (lineage plasticity, contraction efficiency, immunological states, proliferative ability) existing in a spectrum across different individuals and conditions (as reviewed by (desJardins-Park et al., 2018), there is a need to understand how metabolic states influence the wound repair phenotypes. With this, a larger cohort of mammals (rodents from arid habitats) can be screened, possibly creating a spectrum of regenerative ability, with a possibility of different tissue-specific molecular mechanisms, with ROS-reticent (Saxena et al., 2019), highly glycolytic, metabolically plastic, low collagen I-producing, pro-regeneration tissue fibroblasts as the pivotal common denominator.

APPENDIX A: Metabolic response to glucose removal over time.



Supplemental Figure 1. Time is distinctive factor in determining the extent of metabolic homeostatic response to glucose starvation between *Acomys* and *Mus* fibroblasts.

OCR test time course conducted on a Seahorse XF94 analyzer on (a) *Acomys* and (b) *Mus* fibroblasts. ECAR test time course conducted on a Seahorse XF94 analyzer on (c) *Acomys* and (d) *Mus* fibroblasts. Acute glucose starvation involved culturing in glucose deficient media just 24 hours before the Seahorse assay. n=3/species. Measured OCR was converted to percent normalized OCR. FCCP: Carbonyl cyanide-p-trifluoromethoxy phenyl hydrazone.

BIBLIOGRAPHY

- Aztekin, C., & Storer, M. A. (2022). To regenerate or not to regenerate: Vertebrate model organisms of regeneration-competency and -incompetency. *Wound Repair Regen*. doi:10.1111/wrr.13000
- Chetty, S., Pagliuca, F. W., Honore, C., Kweudjeu, A., Rezanian, A., & Melton, D. A. (2013). A simple tool to improve pluripotent stem cell differentiation. *Nat Methods*, *10*(6), 553-556. doi:10.1038/nmeth.2442
- Choi, H. J., Jhe, Y. L., Kim, J., Lim, J. Y., Lee, J. E., Shin, M. K., & Cheong, J. H. (2020). FoxM1-dependent and fatty acid oxidation-mediated ROS modulation is a cell-intrinsic drug resistance mechanism in cancer stem-like cells. *Redox Biol*, *36*, 101589. doi:10.1016/j.redox.2020.101589
- Cook, H., Davies, K. J., Harding, K. G., & Thomas, D. W. (2000). Defective extracellular matrix reorganization by chronic wound fibroblasts is associated with alterations in TIMP-1, TIMP-2, and MMP-2 activity. *J Invest Dermatol*, *115*(2), 225-233. doi:10.1046/j.1523-1747.2000.00044.x
- desJardins-Park, H. E., Foster, D. S., & Longaker, M. T. (2018). Fibroblasts and wound healing: an update. *Regen Med*, *13*(5), 491-495. doi:10.2217/rme-2018-0073
- Folmes, C. D., Nelson, T. J., Martinez-Fernandez, A., Arrell, D. K., Lindor, J. Z., Dzeja, P. P., . . . Terzic, A. (2011). Somatic oxidative bioenergetics transitions into pluripotency-dependent glycolysis to facilitate nuclear reprogramming. *Cell Metab*, *14*(2), 264-271. doi:10.1016/j.cmet.2011.06.011
- Galvao, J., Davis, B., Tilley, M., Normando, E., Duchon, M. R., & Cordeiro, M. F. (2014). Unexpected low-dose toxicity of the universal solvent DMSO. *Faseb j*, *28*(3), 1317-1330. doi:10.1096/fj.13-235440
- Gawriluk, T. R., Simkin, J., Hacker, C. K., Kimani, J. M., Kiama, S. G., Ezenwa, V. O., & Seifert, A. W. (2020). Complex Tissue Regeneration in Mammals Is Associated With Reduced Inflammatory Cytokines and an Influx of T Cells. *Front Immunol*, *11*, 1695. doi:10.3389/fimmu.2020.01695
- Gawriluk, T. R., Simkin, J., Thompson, K. L., Biswas, S. K., Clare-Salzler, Z., Kimani, J. M., . . . Seifert, A. W. (2016). Comparative analysis of ear-hole closure identifies epimorphic regeneration as a discrete trait in mammals. *Nat Commun*, *7*, 11164. doi:10.1038/ncomms11164
- Gomes, L. C., Di Benedetto, G., & Scorrano, L. (2011). During autophagy mitochondria elongate, are spared from degradation and sustain cell viability. *Nat Cell Biol*, *13*(5), 589-598. doi:10.1038/ncb2220
- Hamanaka, R. B., O'Leary, E. M., Witt, L. J., Tian, Y., Gökalp, G. A., Meliton, A. Y., . . . Mutlu, G. M. (2019). Glutamine Metabolism Is Required for Collagen Protein Synthesis

in Lung Fibroblasts. *Am J Respir Cell Mol Biol*, 61(5), 597-606. doi:10.1165/rcmb.2019-0008OC

Huang, C., Murphy, G. F., Akaishi, S., & Ogawa, R. (2013). Keloids and hypertrophic scars: update and future directions. *Plast Reconstr Surg Glob Open*, 1(4), e25. doi:10.1097/GOX.0b013e31829c4597

Lai, S. L., Marín-Juez, R., Moura, P. L., Kuenne, C., Lai, J. K. H., Tsedeke, A. T., . . . Stainier, D. Y. (2017). Reciprocal analyses in zebrafish and medaka reveal that harnessing the immune response promotes cardiac regeneration. *Elife*, 6. doi:10.7554/eLife.25605

Li, S., Chung, H. S., Simakova, A., Wang, Z., Park, S., Fu, L., . . . Matyjaszewski, K. (2017). Biocompatible Polymeric Analogues of DMSO Prepared by Atom Transfer Radical Polymerization. *Biomacromolecules*, 18(2), 475-482. doi:10.1021/acs.biomac.6b01553

Maden, M. (2018). Optimal skin regeneration after full thickness thermal burn injury in the spiny mouse, *Acomys cahirinus*. *Burns*, 44(6), 1509-1520. doi:10.1016/j.burns.2018.05.018

Maden, M., Brant, J. O., Rubiano, A., Sandoval, A. G. W., Simmons, C., Mitchell, R., . . . Patel, K. (2018). Perfect chronic skeletal muscle regeneration in adult spiny mice, *Acomys cahirinus*. *Sci Rep*, 8(1), 8920. doi:10.1038/s41598-018-27178-7

McCusker, C. D., & Gardiner, D. M. (2013). Positional information is reprogrammed in blastema cells of the regenerating limb of the axolotl (*Ambystoma mexicanum*). *PLoS One*, 8(9), e77064. doi:10.1371/journal.pone.0077064

Murphy, M. K., Motz, K. M., Ding, D., Yin, L., Duvvuri, M., Feeley, M., & Hillel, A. T. (2018). Targeting metabolic abnormalities to reverse fibrosis in iatrogenic laryngotracheal stenosis. *Laryngoscope*, 128(2), E59-e67. doi:10.1002/lary.26893

Newsholme, E. A., Crabtree, B., & Ardawi, M. S. (1985). The role of high rates of glycolysis and glutamine utilization in rapidly dividing cells. *Biosci Rep*, 5(5), 393-400. doi:10.1007/bf01116556

Niethammer, P., Grabher, C., Look, A. T., & Mitchison, T. J. (2009). A tissue-scale gradient of hydrogen peroxide mediates rapid wound detection in zebrafish. *Nature*, 459(7249), 996-999. doi:10.1038/nature08119

Nogueira-Rodrigues, J., Leite, S. C., Pinto-Costa, R., Sousa, S. C., Luz, L. L., Sintra, M. A., . . . Sousa, M. M. (2022). Rewired glycosylation activity promotes scarless regeneration and functional recovery in spiny mice after complete spinal cord transection. *Dev Cell*, 57(4), 440-450.e447. doi:10.1016/j.devcel.2021.12.008

Panopoulos, A. D., Yanes, O., Ruiz, S., Kida, Y. S., Diep, D., Tautenhahn, R., . . . Izpisua Belmonte, J. C. (2012). The metabolome of induced pluripotent stem cells reveals

- metabolic changes occurring in somatic cell reprogramming. *Cell Res*, 22(1), 168-177. doi:10.1038/cr.2011.177
- Pinkus, L. M. (1977). Glutamine binding sites. *Methods Enzymol*, 46, 414-427. doi:10.1016/s0076-6879(77)46049-x
- Prigione, A., Fauler, B., Lurz, R., Lehrach, H., & Adjaye, J. (2010). The senescence-related mitochondrial/oxidative stress pathway is repressed in human induced pluripotent stem cells. *Stem Cells*, 28(4), 721-733. doi:10.1002/stem.404
- Rinkevich, Y., Walmsley, G. G., Hu, M. S., Maan, Z. N., Newman, A. M., Drukker, M., . . . Longaker, M. T. (2015). Skin fibrosis. Identification and isolation of a dermal lineage with intrinsic fibrogenic potential. *Science*, 348(6232), aaa2151. doi:10.1126/science.aaa2151
- Sandoval, A. G. W., & Maden, M. (2020). Regeneration in the spiny mouse, *Acomys*, a new mammalian model. *Curr Opin Genet Dev*, 64, 31-36. doi:10.1016/j.gde.2020.05.019
- Saxena, S., Vekaria, H., Sullivan, P. G., & Seifert, A. W. (2019). Connective tissue fibroblasts from highly regenerative mammals are refractory to ROS-induced cellular senescence. *Nat Commun*, 10(1), 4400. doi:10.1038/s41467-019-12398-w
- Seifert, A. W., Kiama, S. G., Seifert, M. G., Goheen, J. R., Palmer, T. M., & Maden, M. (2012). Skin shedding and tissue regeneration in African spiny mice (*Acomys*). *Nature*, 489(7417), 561-565. doi:10.1038/nature11499
- Simkin, J., Gawriluk, T. R., Gensel, J. C., & Seifert, A. W. (2017). Macrophages are necessary for epimorphic regeneration in African spiny mice. *Elife*, 6. doi:10.7554/eLife.24623
- Simkin, J., & Seifert, A. W. (2018). Concise Review: Translating Regenerative Biology into Clinically Relevant Therapies: Are We on the Right Path? *Stem Cells Transl Med*, 7(2), 220-231. doi:10.1002/sctm.17-0213
- Streeter, K. A., Sunshine, M. D., Brant, J. O., Sandoval, A. G. W., Maden, M., & Fuller, D. D. (2020). Molecular and histologic outcomes following spinal cord injury in spiny mice, *Acomys cahirinus*. *J Comp Neurol*, 528(9), 1535-1547. doi:10.1002/cne.24836
- Sumida, K., Igarashi, Y., Toritsuka, N., Matsushita, T., Abe-Tomizawa, K., Aoki, M., . . . Ohno, Y. (2011). Effects of DMSO on gene expression in human and rat hepatocytes. *Hum Exp Toxicol*, 30(10), 1701-1709. doi:10.1177/0960327111399325
- Tsai, H. W., Motz, K. M., Ding, D., Lina, I., Murphy, M. K., Benner, D., . . . Hillel, A. T. (2020). Inhibition of glutaminase to reverse fibrosis in iatrogenic laryngotracheal stenosis. *Laryngoscope*, 130(12), E773-e781. doi:10.1002/lary.28493
- van der Vliet, A., & Janssen-Heininger, Y. M. (2014). Hydrogen peroxide as a damage signal in tissue injury and inflammation: murderer, mediator, or messenger? *J Cell Biochem*, 115(3), 427-435. doi:10.1002/jcb.24683

- Verheijen, M., Lienhard, M., Schrooders, Y., Clayton, O., Nudischer, R., Boerno, S., . . . Caiment, F. (2019). DMSO induces drastic changes in human cellular processes and epigenetic landscape in vitro. *Sci Rep*, *9*(1), 4641. doi:10.1038/s41598-019-40660-0
- Wall, I. B., Moseley, R., Baird, D. M., Kipling, D., Giles, P., Laffafian, I., . . . Stephens, P. (2008). Fibroblast dysfunction is a key factor in the non-healing of chronic venous leg ulcers. *J Invest Dermatol*, *128*(10), 2526-2540. doi:10.1038/jid.2008.114
- Warburg, O. (1956). On the origin of cancer cells. *Science*, *123*(3191), 309-314. doi:10.1126/science.123.3191.309
- Watt, F. M., & Huck, W. T. (2013). Role of the extracellular matrix in regulating stem cell fate. *Nat Rev Mol Cell Biol*, *14*(8), 467-473. doi:10.1038/nrm3620
- Yuan, C., Gao, J., Guo, J., Bai, L., Marshall, C., Cai, Z., . . . Xiao, M. (2014). Dimethyl sulfoxide damages mitochondrial integrity and membrane potential in cultured astrocytes. *PLoS One*, *9*(9), e107447. doi:10.1371/journal.pone.0107447
- Yuan, Y., Yang, Y., Tian, Y., Park, J., Dai, A., Roberts, R. M., . . . Han, X. (2016). Efficient long-term cryopreservation of pluripotent stem cells at -80 °C. *Sci Rep*, *6*, 34476. doi:10.1038/srep34476
- Zhang, J., Nuebel, E., Daley, G. Q., Koehler, C. M., & Teitell, M. A. (2012). Metabolic regulation in pluripotent stem cells during reprogramming and self-renewal. *Cell Stem Cell*,

VITA

1. Ebenezer Nii Adama Aryee
2. BSc. Biochemistry, Cell & Molecular Biology (University of Ghana, Legon)
3. Teaching Assistant (UG: Genetics, Biochemistry lab sessions)
4. Research Assistant (West African Centre for Cell Biology of Infectious Pathogens)
5. Procurement Officer (West African Centre for Cell Biology of Infectious Pathogens)
6. Teaching Assistant (University of Kentucky: Introduction to Biology, Introduction to Evolution recitations)